Beware of commonly used approximations II: estimating systematic biases in the best-fit parameters

José Luis Bernal,[a,b,c] **Nicola Bellomo,**[b,c] **Alvise Raccanelli,**[d,b] **Licia Verde**[b,e]

[a]Department of Physics and Astronomy, Johns Hopkins University, 3400 North Charles Street, Baltimore, Maryland 21218, USA
[b]ICC, University of Barcelona, IEEC-UB, Martí i Franquès, 1, E-08028 Barcelona, Spain.
[c]Dept. de Física Quàntica i Astrofísica, Universitat de Barcelona, Martí i Franquès 1, E-08028 Barcelona, Spain.
[d]Theoretical Physics Department, CERN, 1 Esplanade des Particules, CH-1211 Geneva 23, Switzerland.
[e]ICREA, Pg. Lluis Companys 23, Barcelona, E-08010, Spain.

E-mail: jbernal2@jhu.edu, nicola.bellomo@icc.ub.edu, alvise.raccanelli@cern.ch, liciaverde@icc.ub.edu

Abstract. Cosmological parameter estimation from forthcoming experiments promise to reach much greater precision than current constraints. As statistical errors shrink, the required control over systematic errors increases. Therefore, models or approximations that were sufficiently accurate so far, may introduce significant systematic biases in the parameter best-fit values and jeopardize the robustness of cosmological analyses. We generalize previously proposed expressions to estimate *a priori* the systematic error introduced in parameter inference due to the use of insufficiently good approximations in the computation of the observable of interest or the assumption of an incorrect underlying model. Although this methodology can be applied to measurements of any scientific field, we illustrate its power by studying the effect of modeling the angular galaxy power spectrum incorrectly. We also introduce `Multi_CLASS`, a new, public modification of the Boltzmann code `CLASS`, which includes the possibility to compute angular cross-power spectra for two different tracers. We find that significant biases in most of the cosmological parameters are introduced if one assumes the Limber approximation or neglects lensing magnification in modern galaxy survey analyses, and the effect is in general larger for the multi-tracer case, especially for the parameter controlling primordial non-Gaussianity of the local type, $f_{\rm NL}$.

arXiv:2005.09666v2 [astro-ph.CO] 6 Oct 2020

Contents

1 Introduction

An unprecented experimental and theoretical effort during the last decades has established the Λ-Cold Dark Matter (ΛCDM) model as the standard model of cosmology, because of its striking precision in fitting most of the available observations. This effort has brought forward percent-level constraints on some of the parameters of the model (see e.g., [1–4]). Nonetheless, there are still some remaining tensions between experiments (see e.g., [5–8]) that, in the absence of non-accounted for systematic errors, might hint at the need for an extension of ΛCDM. Forthcoming and future galaxy surveys are expected to push the envelope of observational cosmology on the large scale structure side [9–14], but significant improvements are also expected for CMB experiments [15–17]. Moreover, the advent of line-intensity mapping experiments [18, 19] with its potential for cosmology (see e.g., [20]) promises to open a window to explore the Universe at higher redshift and close the gap between CMB and galaxy surveys observations (see e.g., [21, 22]).

The aim of these experiments is to achieve subpercent-level precision for parameter inference within ΛCDM and to further constrain (and possibly even detect) deviations from ΛCDM. The promising capabilities of these experiments will make possible a dramatic reduction of the statistical errors: expected statistical uncertainties are well below the current systematic error budget. Therefore, it is of crucial importance to maintain systematic biases below the statistical errors as well as a correct assessment of the final, true uncertainties. Accurate modeling of the target observables is one of the key ingredients needed in order to succeed in this challenge. However, higher accuracy often requires more complicated and

expensive modeling. This can be mitigated by introducing careful approximations in the modeling of the signal and their covariances to speed up calculations without significant reductions in accuracy.

Using insufficiently accurate approximations in the analysis affects the inferred model parameters in two ways. First, it may shift the point in parameter space where the posterior distribution peaks, which would introduce a systematic bias in the best-fit parameters. Second, the shape of the posterior distribution may be affected, yielding a misestimate of the uncertainties. In summary, these two effects can be understood as errors in the parameters values and in their error-bars. Therefore, the effects on the posterior (in terms of potential shifts of the best-fit parameters and their errors) of any approximation to be adopted must be estimated quantitatively in light of the forecasted experimental performance. Moreover, a theoretical systematic error might be introduced even if the modeling of the observable is accurate enough, when the underlying cosmological model assumed is incorrect: the inferred cosmological parameters assuming ΛCDM will be most likely biased if the Universe is better described by a different model.

We approach the estimation of the bias in the best-fit parameters in the same spirit of previous works focusing on specific problems in cosmology. Some studies focused on the bias introduced by assuming an incorrect cosmological model M_1 instead of the correct one M_0, where M_1 and M_0 are nested models [23]. The general expression for nested models can be found in Refs. [24, 25], where it was used to estimate the impact of not marginalizing over a subset of nuisance parameters. Others investigated the bias arising from an incorrect modeling of the target observable for several specific cases, including the impact of inhomogeneous reionization on CMB anisotropies [26], the effect on weak lensing measurements from incorrect modeling of the non linear power spectrum and galaxy redshift distribution [27, 28], observational systematics [29, 30] or baryonic feedback [31], SN magnitudes [32], the modeling of redshift-space distortions of the galaxy power spectrum [33], emission-line galaxy power spectrum measurements without including the contamination due to line interlopers [34], the contribution of relativistic effects on galaxy surveys [35–38], and the neutrino-induced scale-dependence of the galaxy bias [39]. There are also studies focused on how parameter inference is affected by misestimations of the covariance matrices (see e.g., [40, 41]) or the use of an invalid likelihood (see e.g., [42, 43]).

Instead, in this work we aim to generalize the methodology to be applicable to any observable, not necessarily in cosmology. There are two different causes that lead to parameter biases: the assumption of an incorrect model (e.g., assuming a cosmological constant in the case dark energy is dynamical) and the use of an incorrect or incomplete modeling of the observable considered (e.g., using an inaccurate modeling of the redshift-space distortions). Although the previous studies mentioned above considered only one of them, these two causes may be interdependent. Our approach treats both of them on the same footing, accounting for any possible interaction between them.

Our approach can be summarized as follows. We consider data drawn from an underlying model. Then, we expand the theoretical prediction of the observable, computed according to a given model under study, around a fiducial set of parameters. Note that the model under study is not necessarily the same model the data are drawn from. Subsequently, we apply this expansion to the likelihood of the observable, maximize such likelihood, and obtain the best-fit value of the parameters. We follow this procedure in two cases: a correct description of the observable and an approximated one. From here, we estimate the systematic bias comparing the best-fit parameters obtained in both cases.

This technique, as is the case for Fisher matrix analyses, is conceived to be used prior to obtaining data. In this case, it is required to choose a model as a good representation of reality and compute the data according to it. Employing our approach before the data is obtained will allow for the determination of the level of accuracy needed in the data analysis of an experiment during its design. Moreover, it will help to quantify the significance of new contributions or corrections to the theoretical modeling of the signal in light of the potential of future experiments. Nonetheless, the methodology can also be applied to actual observations to ascertain whether a more numerically intensive modeling is needed.

We demonstrate the power of our approach by applying it to the angular galaxy power spectrum. We primarily focus on the systematic shifts of the best-fit parameters, whereas the misestimation of the uncertainties in parameter inference is studied in a companion paper [44], hereinafter Paper I. Besides traditional, single-tracer analysis, we also consider multi-tracer analyses of the galaxy clustering. We present two practical examples: we explore how neglecting cosmic magnification or using the Limber approximation may introduce significant systematic biases ($\gtrsim 1 - 2\sigma$ in most of the parameters and cases under study) in the analyses of next-generation galaxy surveys.

We also present and publish `Multi_CLASS`. [1] `Multi_CLASS` is a modification of the public Boltzmann code CLASS [45, 46] that allows for the computation of the angular cross-power spectra of two different tracers of the underlying density field, with their corresponding different redshift dependence of the tracer characteristics (bias, magnification bias, evolution bias and number density distribution). This possibility enables comprehensive theoretical multi-tracer analyses. Furthermore, it includes an implementation for primordial non-Gaussianities of the local type, parametrized by the $f_{\rm NL}$ parameter, on the clustering observables. More details about the options and implementation of `Multi_CLASS` can be found in Appendix B of Paper I.

This paper is organized as follows: we generalize the methodology to estimate the bias introduced in best-fit parameters by an inaccurate modeling of a given measurement in Section 2; introduce our test-case, the angular galaxy power spectrum, and our assumptions for the demonstration of the potential of our approach in Section 3; show the estimated systematic bias introduced in cosmological parameter inference by using the angular galaxy power spectrum without modeling lensing magnification or applying the Limber approximation in Section 4; and conclude in Section 5. Appendix A contains an evaluation of the performance of the estimation of the bias, the derivation of the estimated bias expanding the observable up to second order on the model parameters, and a discussion of likelihoods of Wishart-distributed variables. Appendix B quantifies the dependence of the bias in the best-fit parameters on the largest scales included in the angular galaxy power spectrum analysis.

2 Systematic shift of the best-fit parameters due to incorrect modeling

We begin by defining notation and conventions. We use vector operators for quantities in parameter space; operations involving the observable space (e.g., the data vector or its covariance) are explicitly written down as sums over the matrix elements. Unless otherwise stated, all vectors are column vectors. For the sake of clarity, the meaning of all symbols, superscripts and subscripts used in this section can be consulted in Table 1.

---

[1] `Multi_CLASS` will be publicly available in https://github.com/nbellomo/Multi_CLASS upon the acceptance of this work.

Symbol	Meaning	Super/sub-script	Meaning
M	Underlying model	d	Data
$\boldsymbol{\theta}$	Set of model's parameters	ˆ	Theoretical prediction
Ψ	Observable	i/j	Components of the observable's vector
Cov	Observable's covariance	$\star$	Generic point in parameter space
$\mathcal{L}$	Likelihood	θ	In parameter space
$\Delta\boldsymbol{\theta}$	Finite difference in parameter space	0	Related to the true underlying model
F	Fisher matrix	tr	Actual value in reality
$\boldsymbol{\Delta}_{\mathrm{syst}}$	Systematic bias on parameters	fid	Assumed fiducial value
		bf	Best-fit value
		a/b	Components of the parameter's vector
		C	Computed under correct assumptions/approximations
		I	Computed under incorrect assumptions/approximations
		α	Related to an individual likelihood

Table 1: Table for reference with the meaning of each of the symbols, subscripts and superscripts used in Section 2.

Let us consider a generic model M specified by a set of parameters $\boldsymbol{\theta}$ that, according to some theoretical modeling, determine the observable Ψ and its covariance Cov. While in principle there is no need to distinguish between model and modeling, this is useful in some cases, like for instance, cosmology, where 'model' usually refers to the cosmological model (e.g., ΛCDM) and 'modeling' refers to the practical application of the model to describe the observables under study. In the case of cosmology, for example, there is a much wider variety of modeling approaches than of models. Assuming a Gaussian likelihood for Ψ (which usually is a good approximation close to its maximum, or in case the central limit theorem applies), the logarithm of the likelihood given M depends on $\boldsymbol{\theta}$ as

$$
\begin{aligned}
-2\log\mathcal{L}\left(\Psi^{\mathrm{d}}|M,\boldsymbol{\theta}\right) &= \\
&= \sum_{i,j}\left(\Psi_i^{\mathrm{d}}-\hat{\Psi}_i(\boldsymbol{\theta})\right)\left(\mathrm{Cov}^{-1}(\boldsymbol{\theta})\right)_{ij}\left(\Psi_j^{\mathrm{d}}-\hat{\Psi}_j(\boldsymbol{\theta})\right)^* + \log|\mathrm{Cov}(\boldsymbol{\theta})| ,
\end{aligned}
\tag{2.1}
$$

where Ψ^{d} and $\hat{\Psi}(\boldsymbol{\theta})\equiv\hat{\Psi}(\boldsymbol{\theta}|M)$ are the data vector and the corresponding theoretical prediction of the observable, respectively, i and j denote vector and matrix indices, and the superscript '*' indicates the complex conjugate operation. The constant terms in $\log\mathcal{L}$, which are not included in Equation (2.1), do not affect parameter inference, hence we neglect them throughout this work. In the following, we assume real quantities for Ψ in order to drop the notation referring to the complex conjugate. Nonetheless, we stress that our derivation is equally valid to complex observables.

Equation (2.1) considers the general case in which the covariance is not fixed but varies as function of the model parameters. For simplicity, in what follows we assume a fixed covariance (i.e., computed for a fiducial model with a specific choice of parameter values). Hence, the second term of the right hand side of Equation (2.1) is constant, and can be removed from the equation. It is straightforward to extend the methodology to the case of a parameter-dependent covariance matrix following the steps detailed below. Hereinafter we drop the explicit notation for the dependence on the parameters of the model.

For a specific set of parameters $\boldsymbol{\theta}^\star$ within a given model, our target observable is $\hat{\Psi}^\star = \hat{\Psi}(\boldsymbol{\theta}^\star)$. We can approximate the value of the observable under any small variation of the model parameters around $\boldsymbol{\theta}^\star$ expanding to linear order as

$$\hat{\Psi}_i(\boldsymbol{\theta}^\star + \Delta\boldsymbol{\theta}) \approx \hat{\Psi}_i^\star + \left(\boldsymbol{\nabla}_\theta \hat{\Psi}_i^\star\right)^T \Delta\boldsymbol{\theta}, \tag{2.2}$$

where $\boldsymbol{\nabla}_\theta$ denotes the gradient operator with respect to the model parameters, the superscript 'T' denotes the transpose operator, and $\Delta\boldsymbol{\theta}$ is a small finite difference in the parameters space. This approximation is exact when $\hat{\Psi}$ depends linearly on $\boldsymbol{\theta}$; otherwise, its accuracy decreases as $\Delta\boldsymbol{\theta}$ increases.

Let us assume that M_0, with parameters $\boldsymbol{\theta}_0$, is the true underlying model for the phenomenon of interest. Then, Ψ^{d} corresponds to a realization of M_0 given $\boldsymbol{\theta}_0^{\mathrm{tr}}$, with $\hat{\Psi}(\boldsymbol{\theta}_0^{\mathrm{tr}}) = \langle\Psi^{\mathrm{d}}\rangle$, where the superscript 'tr' refers to the parameter values corresponding to reality and the brackets $\langle\cdot\rangle$ refer to the ensemble average. [2] This is true in practice only if Ψ^{d} is not contaminated with unaccounted-for systematics and an exact theoretical modeling is used to compute $\hat{\Psi}(\boldsymbol{\theta}_0^{\mathrm{tr}})$ and its covariance. On the other hand, we can consider a fiducial set of parameters $\boldsymbol{\theta}^{\mathrm{fid}}$ within M guessed to be close to the point in parameter space where the likelihood peaks (e.g., inferred from prior or complementary experiments). Note that M and $\boldsymbol{\theta}^{\mathrm{fid}}$ do not need to be the same model and parameters as M_0 and $\boldsymbol{\theta}_0^{\mathrm{tr}}$; then, in the most general case, we have $\hat{\Psi}(\boldsymbol{\theta}^{\mathrm{fid}}|M) = \hat{\Psi}^{\mathrm{fid}} \neq \Psi^{\mathrm{d}}$. We can expand $\hat{\Psi}^{\mathrm{fid}}$ using Equation (2.2), apply it to Equation (2.1) and maximize the likelihood to obtain the best-fit parameters $\boldsymbol{\theta}^{\mathrm{bf}}$ for the model M. After the maximization, we have

$$\sum_{i,j} \left(\boldsymbol{\nabla}_\theta \hat{\Psi}_i^{\mathrm{fid}}\right) \left(\mathrm{Cov}^{-1}\right)_{ij} \left[\Psi_j^{\mathrm{d}} - \hat{\Psi}_j^{\mathrm{fid}} - \left(\boldsymbol{\nabla}_\theta \hat{\Psi}_j^{\mathrm{fid}}\right)^T \Delta\boldsymbol{\theta}\right] = 0 \longrightarrow$$
$$\sum_{i,j} \left(\boldsymbol{\nabla}_\theta \hat{\Psi}_i^{\mathrm{fid}}\right) \left(\mathrm{Cov}^{-1}\right)_{ij} \left(\Psi_j^{\mathrm{d}} - \hat{\Psi}_j^{\mathrm{fid}}\right) = \sum_{i,j} \left(\boldsymbol{\nabla}_\theta \hat{\Psi}_i^{\mathrm{fid}}\right) \left(\mathrm{Cov}^{-1}\right)_{ij} \left(\boldsymbol{\nabla}_\theta \hat{\Psi}_j^{\mathrm{fid}}\right)^T \Delta\boldsymbol{\theta}, \tag{2.3}$$

where we have neglected all derivatives of order higher than one. Solving Equation (2.3) for $\Delta\boldsymbol{\theta}$ returns the step in parameter space needed in order to maximize the likelihood: $\Delta\boldsymbol{\theta} \equiv \boldsymbol{\theta}^{\mathrm{bf}} - \boldsymbol{\theta}^{\mathrm{fid}}$. The factor multiplying $\Delta\boldsymbol{\theta}$ in the right-hand side of Equation (2.3) can be identified as the Gaussian Fisher information matrix, whose elements are given by [47]

$$F_{a,b} = \left\langle \frac{\partial^2 \log \mathcal{L}}{\partial\theta_a \partial\theta_b} \right\rangle = \sum_{i,j} \left(\frac{\partial\hat{\Psi}_i^{\mathrm{fid}}}{\partial\theta_a}\right) \left(\mathrm{Cov}^{-1}\right)_{ij} \left(\frac{\partial\hat{\Psi}_j^{\mathrm{fid}}}{\partial\theta_b}\right), \tag{2.4}$$

where a and b refer to indices of the parameters vector. Therefore, we can estimate the difference between the best-fit parameters and the fiducial parameters initially assumed as

$$\Delta\boldsymbol{\theta} \equiv \boldsymbol{\theta}^{\mathrm{bf}} - \boldsymbol{\theta}^{\mathrm{fid}} = F^{-1} \sum_{i,j} \left(\boldsymbol{\nabla}_\theta \hat{\Psi}_i^{\mathrm{fid}}\right) \left(\mathrm{Cov}^{-1}\right)_{ij} \left(\Psi_j^{\mathrm{d}} - \hat{\Psi}_j^{\mathrm{fid}}\right). \tag{2.5}$$

Of course, if M is a good approximation of M_0 and the modeling used to compute $\hat{\Psi}^{\mathrm{fid}}$ is accurate, $\boldsymbol{\theta}^{\mathrm{bf}}$ will be very close to $\boldsymbol{\theta}_0^{\mathrm{tr}}$.

---

[2] In certain cases, like in cosmology, it is not always possible to obtain a meaningful ensemble average. In this scenario, we assume that $\boldsymbol{\theta}^{\mathrm{tr}}$ represent a faithful reproduction of the observed realization.

We can apply the same procedure to a joint analysis of several likelihoods, corresponding to different observables, experiments or independent data sets. However, it is important to note that in general the global best-fit parameters $\boldsymbol{\theta}^{\mathrm{bf}}$ are different than the best-fit values $\boldsymbol{\theta}^{\mathrm{bf}}_{\alpha}$ for each independent likelihood. Let us consider independent likelihoods, so that the joint likelihood is the product of the individual likelihoods $\mathcal{L}_{\alpha}$ (i.e., $\log \mathcal{L} = \sum_{\alpha} \log \mathcal{L}_{\alpha}$). In this scenario, Equation (2.5) is generalized as

$$\Delta\boldsymbol{\theta} = \left(\sum_{\alpha} F_{\alpha}\right)^{-1} \left[\sum_{\alpha,i,j} \left(\boldsymbol{\nabla}_{\theta}\hat{\Psi}^{\mathrm{fid}}_{\alpha;i}\right) \left(\mathrm{Cov}_{\alpha}^{-1}\right)_{ij} \left(\Psi^{\mathrm{d}}_{\alpha;j} - \hat{\Psi}^{\mathrm{fid}}_{\alpha;j}\right)\right], \qquad (2.6)$$

where we denote quantities referred to individual likelihoods with the subscript α (i.e., $\Psi_{\alpha;i}$ refers to the i-th element of the observable corresponding to the α-th likelihood). If the likelihoods involved in the joint analysis have different nuisance parameters, F_{α} should be marginalized over the nuisance parameters not common between likelihoods, which will not be included in the parameters vector $\boldsymbol{\theta}_{\alpha}$. Equation (2.6) can be straightforwardly generalized to non-independent likelihoods accounting for their covariance in the computation of both the Fisher matrix and the factor in square brackets.

Taking all this into account, we are now ready to compare the performance of a correct and an incorrect modeling of the observable, as well as the effects of assuming an incorrect underlying model. We assume, as before, that Ψ^{d} is drawn from model M_0, but this model is unknown. We also consider two theoretical predictions of the observable, $\hat{\Psi}^{\mathrm{C}}$ and $\hat{\Psi}^{\mathrm{I}}$, which differ in the set of assumptions and approximations made for its modeling and in the model assumed: $\hat{\Psi}^{\mathrm{C}}$ (correct) uses an accurate and precise modeling assuming a correct model M^{C}, while insufficiently good approximations are implemented, incorrect assumptions are adopted, or an imperfect model M^{I} is used to compute $\hat{\Psi}^{\mathrm{I}}$ (incorrect). We can estimate the systematic error $\boldsymbol{\Delta}_{\mathrm{syst}}$ induced by using $\hat{\Psi}^{\mathrm{I}}$ instead of $\hat{\Psi}^{\mathrm{C}}$ as

$$\boldsymbol{\Delta}_{\mathrm{syst}} \equiv \boldsymbol{\theta}^{\mathrm{bf,I}} - \boldsymbol{\theta}^{\mathrm{bf,C}}, \qquad (2.7)$$

where $\boldsymbol{\theta}^{\mathrm{bf,I}}$ and $\boldsymbol{\theta}^{\mathrm{bf,C}}$ are obtained using Equation (2.3) for the correct and incorrect cases introduced above.

Our approach to estimate the bias in the inferred parameters can be applied both to real measurements and before they are obtained. As said above, the latter case requires the assumption of a model M_0 with true parameters $\boldsymbol{\theta}^{\mathrm{tr}}_0$ as the perfect description of reality; in most forecasts, the assumed fiducial model for the analysis is considered to perfectly describe future observations, hence $\Psi^{\mathrm{d}} = \hat{\Psi}^{\mathrm{fid,C}}$.

To make Equation (2.7) consistent, if M^{C} and M^{I} are nested models, the parameter space of the model with less parameters should be considered as a hyperplane of the parameter space of the other model, with the values of the extra parameters being kept fixed. Consider that θ_a is the extra parameter. In this case, for the model with less parameters we have $\partial\hat{\Psi}/\partial\theta_a = 0$. In order to model that this parameter is fixed in the Fisher matrix (and have the same number of parameters in the vectors that enter Equation (2.7)), we enforce $F_{*,a} = F_{a,*} \to \infty$, where the subscript $*$ refer to all indices of the parameters vector. This is equivalent to have a perfect prior on θ_a.

Equations (2.5), (2.6) and (2.7) are a generalization of other expressions that have been introduced before for specific cases (see e.g. [23–39]). Our expressions, on the contrary, can be applied to the analysis of any given observable, also prior to its measurement. These

expressions allows one to estimate the impact of modeling assumptions and approximations as well as incorrect choices of the underlying model on the inferred parameters. We envision that it will also be useful to single out possible sources of systematic errors affecting new or unexpected findings.

As stated above, the expansion of the observable up to linear order on $\Delta\boldsymbol{\theta}$ (Equation (2.2)) is less and less accurate as $\Delta\boldsymbol{\theta}$ increases (unless the observable is actually linear on $\Delta\boldsymbol{\theta}$). Therefore, in the case the bias introduced on parameter inference is very large, Equation (2.5) provides only rough estimations. Of course the estimate of a large bias, even if quantitatively not accurate, is a clear 'red flag' for the adoption of the approximation under consideration, hence the approach is still useful. Nevertheless we further quantify the accuracy of the shift in the parameters estimated with Eqs. (2.5), (2.6), (2.7). In Appendix A, we evaluate the performance of the approach outlined in the main text here for a specific case of our case example, the angular galaxy power spectrum. Moreover, we also discuss how this approach can be made even more accurate in this appendix. Although we use the linear expansion discussed in this section in the main body of the text, we derive the estimation of $\Delta\boldsymbol{\theta}$ for an expansion of $\hat{\Psi}$ up to second order in $\Delta\boldsymbol{\theta}$. Finally, we also discuss the estimation of $\Delta\boldsymbol{\theta}$ assuming a likelihood of Wishart-distributed variables, as it is the case of the angular galaxy power spectrum.

3 Observable and cosmological model considered

Although the methodology described above is valid for any measurement, here we focus on its application to cosmology. Given the vast amount of observed data and the complexity of some theoretical calculations, theoretical and numerical approximations are very common. Assessing the reliability of different assumptions might be challenging, but not doing it might have unacceptable consequences. Concretely, we consider the angular galaxy power spectrum as our target observable. The dramatic improvement in the quality of the observations will require a much better modeling in order to fully exploit coming galaxy surveys. Therefore, approximations that were commonly used in studies about galaxy clustering might not be accurate anymore. Some of these approximations include, but are not limited to: neglecting relativistic corrections, the Limber approximation, an incorrect estimation of the covariance matrix, a poor modeling of non-linear clustering and specific approximations used to model observational effects. For illustrative purposes, in this work we focus on the two first approximations of this list. In Paper I, where the focus is set on the misestimation of the parameter uncertainties, we also study the consequences of neglecting the covariance between different redshifts bins. However, this is expected to have limited impact on the best-fit parameter values; hence, we do not consider this approximation in this study.

The modeling of the angular power spectrum and of the associated likelihood is discussed with detail in Paper I; here we describe it only briefly, and encourage the reader to refer to Paper I for a full description. The observed galaxy number count perturbations receive contributions from the intrinsic galaxy overdensities as well as from other effects, such as redshift-space distortions due to peculiar velocities or lensing effects caused by density perturbations along the line of sight. [3] All these effects can be modeled in harmonic space introducing several transfer functions, the combined effect of which is given by the

---

[3]Observational effects (e.g., the observational mask) also modify the observed galaxy overdensity. However, their modeling is extremely case dependent, and will be presented elsewhere. Since we are interested in differential effects, neglecting this is not expected to affect our findings.

total transfer function $\Delta_\ell^X(k, z)$ as function of wave number k and redshift z, where ℓ is the corresponding multipole and X refers to the tracer considered. The explicit form of the contributions from intrinsic clustering, peculiar velocities and relativistic corrections to Δ_ℓ^X can be found in Appendix A of Paper I. Δ_ℓ^X can be restricted to a given redshift bin applying a window function $W(z, z_X, \Delta z_X)$ centered at z_X, the width of which is controlled by Δz_X. For instance, Δz_X often refers to the half-width or the standard deviation of a top-hat or a Gaussian window function, respectively. Accounting for the number density of galaxies per redshift dN_X/dz, the transfer function for a specific redshift bin can be expressed as

$$\Delta_\ell^{X,z_X}(k) = \int_0^\infty dz \frac{dN_X}{dz} W(z, z_X, \Delta z_X) \Delta_\ell^X(k, z), \tag{3.1}$$

where the integral of $W(z, z_X, \Delta z_X) dN_X/dz$ is equal to unity. Spectroscopic galaxy surveys provide very precise redshifts for each galaxy included in the catalog. On the contrary, photometric galaxy surveys sacrifice the precision in the redshift measurements for the sake of observing more galaxies. This uncertainty in the radial position of the galaxies is usually modeled as a smoothing in the radial component of the three-dimensional clustering in configuration space at small scales. However, the modeling of photometric redshift uncertainties for the angular clustering statistics can be embedded in the choice of window function, given that the radial clustering is projected. Photometric redshifts make impossible to use sharp and narrow redshift bins: the most common choice is to use Gaussian window functions.

With these conventions, the linear angular galaxy power spectrum for tracers X and Y and redshift bins z_X and z_Y, respectively, is given by

$$C_\ell^{XY}(z_X, z_Y) = 4\pi \int \frac{dk}{k} \mathcal{P}_0(k) \Delta_\ell^{X,z_X}(k) \Delta_\ell^{Y,z_Y}(k), \tag{3.2}$$

where $\mathcal{P}_0(k) = k^3 P_0(k)/2\pi^2$ is the adimensional, almost scale-invariant, power-law primordial power spectrum of scalar curvature perturbations.

Galaxies are discrete tracers of the underlying density fluctuations, and therefore their power spectra are affected by shot noise. We assume a Poissonian scale-independent shot noise contribution to be added to the theoretical angular galaxy power spectrum computed in Equation (3.2), hence the total angular power spectrum can be defined as

$$\tilde{C}_\ell^{XY}(z_X, z_Y) = C_\ell^{XY}(z_X, z_Y) + \frac{\delta_{z_X z_Y}^K \delta_{XY}^K}{dN_X(z_X)/d\Omega}, \tag{3.3}$$

where $dN_X(z_X)/d\Omega$ is the mean number density per steradian for tracer X in the redshift bin centered at z_X, and δ^K is a Kronecker delta. Note that with these assumptions the shot noise term only contributes to the total power spectrum for the auto-power spectrum (i.e., same redshift bin and same tracer). Nonetheless, the shot noise might have non-Poissonian contributions (see e.g. [48, 49]). Furthermore, theoretical uncertainties can be added as noise, especially those regarding non-linear scales (see e.g., [50]).

We want to consider all possible combinations of tracers and redshift bins, and denote the number of redshift bins for tracer X and Y with N_X and N_Y, respectively. As explained in detail in Paper I, one can consider the angular power spectra or the spherical harmonics coefficients of the galaxy number count fluctuations as the data vector. Depending on the choice, the theoretical $\tilde{C}_\ell$ are used in different manners. For the first option, the power spectra between different redshift bins and tracers at a given multipole are placed in a vector

$\boldsymbol{C}_\ell$ of size $N_X(N_X + 1)/2 + N_Y(N_Y + 1)/2 + N_X N_Y$. In turn, for the second option, they form matrices $\mathcal{C}_\ell$ of size $(N_X + N_Y) \times (N_X + N_Y)$ which represent the covariance between the spherical harmonic coefficients. Hence, there is a $\boldsymbol{C}_\ell$ vector and a $\mathcal{C}_\ell$ matrix for each multipole ℓ. This choice also determines how the elements of the Fisher matrix are computed [51]:

$$
\begin{aligned}
F_{ab} &= \sum_{\ell,i,j} \left(\frac{\partial C_\ell}{\partial \theta_a} \right)_i \left(\mathcal{M}_\ell^{-1} \right)_{ij} \left(\frac{\partial C_\ell}{\partial \theta_b} \right)_j = \\
&= f_{\text{sky}} \sum_\ell \frac{2\ell + 1}{2} \sum_{p,q,r,s} \left(\frac{\partial \mathcal{C}_\ell}{\partial \theta_a} \right)_{pq} \left(\mathcal{C}_\ell^{-1} \right)_{qr} \left(\frac{\partial \mathcal{C}_\ell}{\partial \theta_b} \right)_{rs} \left(\mathcal{C}_\ell^{-1} \right)_{sp} ,
\end{aligned}
\tag{3.4}
$$

where f_{sky} is the fraction of the sky probed by the survey, $\mathcal{M}_\ell$ is a matrix representing the covariance between the elements of $\boldsymbol{C}_\ell$, indicated by the indices i and j. In the second line of Equation (3.4), p, q, r and s refer to the indices of $\mathcal{C}_\ell$; in the sum over these indices, one can recognise the trace of the product of the four matrices involved. We refer the interested reader to Appendix A of Ref. [52] for further details on the derivation of this expression and the matrix properties used. The index i of $\boldsymbol{C}_\ell$ corresponds to $\tilde{C}_\ell^{(i_1, i_2)} \equiv \tilde{C}_\ell^{XY}(z_X, z_Y)$, where i_1 and i_2 specify each unique combination of X and z_X and Y and z_Y, respectively, of the transfer functions involved in Equation (3.2). Then, each element i, j of the covariance matrix $\mathcal{M}_\ell$ is given by

$$
(\mathcal{M}_\ell)_{ij} = \frac{1}{f_{\text{sky}} (2\ell + 1)} \left(\tilde{C}_\ell^{(i_1 j_1)} \tilde{C}_\ell^{(i_2 j_2)} + \tilde{C}_\ell^{(i_1 j_2)} \tilde{C}_\ell^{(i_2 j_1)} \right).
\tag{3.5}
$$

Now that we have specified the target observable, its covariance, and its Fisher matrix, we can explicitly apply the formalism described in Section 2. In this case, we can identify the data and theory vector Ψ as $\boldsymbol{C}_\ell$, and its covariance is given by $\mathcal{M}_\ell$. Specifying the general expression in Equation (2.5) to the case of the angular galaxy power spectra we obtain that the difference between the best-fit parameters and the initially assumed fiducial parameters within a general model is

$$
\begin{aligned}
\Delta\boldsymbol{\theta} &= \boldsymbol{\theta}^{\text{bf}} - \boldsymbol{\theta}^{\text{fid}} = F^{-1} \sum_{\ell,i,j} \left(\boldsymbol{\nabla}_\theta C_\ell^{\text{fid}} \right)_i \left(\mathcal{M}_\ell^{-1} \right)_{ij} \left(C_\ell^{\text{d}} - C_\ell^{\text{fid}} \right)_j = \\
&= F^{-1} f_{\text{sky}} \sum_\ell \frac{2\ell + 1}{2} \sum_{p,q,r,s} \left(\boldsymbol{\nabla}_\theta \mathcal{C}_\ell^{\text{fid}} \right)_{pq} \left[\left(\mathcal{C}_\ell^{\text{fid}} \right)^{-1} \right]_{qr} \left(\mathcal{C}_\ell^{\text{d}} - \mathcal{C}_\ell^{\text{fid}} \right)_{rs} \left[(\mathcal{C}_\ell^{\text{fid}})^{-1} \right]_{sp} .
\end{aligned}
\tag{3.6}
$$

Equation (3.6) can be applied to the correct description of the angular galaxy power spectra and to an approximated one. The substitution of these results in Equation (2.7) yields the systematic bias introduced in parameter inference due to the approximated description, $\boldsymbol{\Delta}_{\text{syst}}$.

As pointed out in Paper I, Equation (3.4) is only valid in the case that the same multipole range is used for all redshift bins. This is because both $\mathcal{M}_\ell$ and $\mathcal{C}_\ell$ would be singular otherwise: the matrices corresponding to the multipoles that are not used in all redshift bins would contain complete rows and columns filled with zeros. Therefore, Equation (3.4) cannot be applied when the maximum multipole used depends on redshift. This would be the case, for instance, of modeling the redshift dependence of the scales for which non-linear clustering becomes significant. However, one can consider different likelihoods using a different multipole range for each of them in order to overcome this limitation. Each of these

likelihoods includes only the power spectra between the redshift bins that cover the corresponding multipole range. We refer the interested reader to Paper I for more details. Taking this into account, it is straightforward to generalize Equation (3.6) to this case comparing Equations (2.5) and Equation (2.6).

3.1 Cosmological model under study and straw-man survey examples

Given the promising prospects of future galaxy surveys to constrain primordial non-Gaussianities (see e.g., [11, 13, 53–57]), we choose ΛCDM+$f_{\rm NL}$ to be the cosmological model under study, where $f_{\rm NL}$ parametrizes the amplitude of primordial non-Gaussianity of the local type controlling the amplitude of the quadractic contributions of a Gaussian random field to the Bardeen potential. The effect of this type of non-Gaussianity on the clustering of halos can be modeled with a strong scale-dependence of the galaxy bias on large scales [58–61]. Denoting the standard, scale-independent Gaussian galaxy bias as b_G and using the large-scale structure convention for $f_{\rm NL}$, the total galaxy bias is given by

$$b_{\rm tot}(k, z) = b_G + (b_G - 1)f_{\rm NL}\delta_{\rm crit}\frac{3\Omega_{\rm m}H_0^2}{c^2 k^2 T(k, z)}, \tag{3.7}$$

where $\delta_{\rm crit} = 1.68$ is the critical density related with spherical gravitational collapse in an Einstein-de Sitter cosmology, $\Omega_{\rm m}$ is the matter density parameter today, H_0 is the Hubble constant, c is the speed of light, and $T(k, z)$ is the transfer function of matter.[4]

Including the Gaussian galaxy bias of each tracer as a model parameter, the set of parameters considered in this work to model ΛCDM+$f_{\rm NL}$ is $\boldsymbol{\theta} = \left\{h, \omega_{\rm b}, \omega_{\rm cdm}, n_{\rm s}, b_G^X, b_G^Y, f_{\rm NL}\right\}$,[5] where $\omega_{\rm b}$ and $\omega_{\rm cdm}$ are the physical densities of baryons and cold dark matter, respectively, n_s is the spectral index of $\mathcal{P}_0(k)$, and b_G^X (b_G^Y) is the Gaussian galaxy bias for the tracer X (Y). Note that for analyses with only one tracer, b_G^X and b_G^Y become simply b_G.

As done in Paper I, we consider three straw-man galaxy surveys to study if the systematic biases depend qualitatively on the survey parameters, as well as to study the multi-tracer case. First, we consider a survey with galaxies uniformly distributed in redshift and a galaxy density per unit redshift and square degree $d^2N_{\rm g}/dzd\Omega = 1070$ gal/deg^2. We also consider two other more realistic surveys, inspired by the galaxy redshift distribution expected for Euclid [11] (in a pessimistic scenario) and SPHEREx [14], which we approximate by

$$\frac{d^2N}{dzd\Omega} = A\left(\frac{z}{z_0}\right)^\alpha e^{-(z/z_0)^{1.5}} \text{gal/deg}^2, \tag{3.8}$$

with $A^{\rm Eu-l} = 2.4 \times 10^3$, $z_0^{\rm Eu-l} = 0.54$, and $\alpha^{\rm Eu-l} = 4.0$ for Euclid; and $A^{\rm SP-l} = 2.93 \times 10^4$, $z_0^{\rm SP-l} = 0.53$ and $\alpha^{\rm SP-l} = 1.1$. We denote these two galaxy distributions as Euclid-like and SPHEREx-like, respectively, with corresponding related superscripts 'Eu-l' and 'SP-l'. We normalize the number density of the uniformly sampled survey to contain the same number of galaxies as our Euclid-like survey.

We consider a full redshift range $0.1 \leq z \leq 2.1(2.2)$, split into five redshift bins centered at $z = 0.3, 0.7, 1.1, 1.5$, and 1.9 for the three galaxy surveys considered. All redshift bins

---

[4]Detailed comparison with N-body simulations indicate that there might be a correction factor of order unity to Equation (3.7) (see e.g., [62, 63]), which for simplicity we omit here. Hence, $f_{\rm NL}$ in Equation (3.7) should be considered as an effective primordial non-Gaussianity parameter of about the same magnitude of the true underlying $f_{\rm NL}$.

[5]We do not consider the amplitude of $\mathcal{P}_0$ as a free parameter in our analysis because it is almost completely degenerate with b_G^X and b_G^Y, although we are aware that it should be included in an analysis of real observations.

have a top-hat window function with half-widths of 0.2 or 0.3 (so that the redshift window functions of adjacent redshift bins overlap only in the second case); we refer to these two cases as 'non-overlap' and 'overlap' cases, respectively. The overlapping case with top-hat window functions can be understood as a worst-case scenario for limited photometric redshift uncertainties. While Gaussian window functions overlap with each other, it is the non-overlapping intervals which contribute the most to the angular power spectrum (see Equation (3.1)). On the other hand, top-hat window functions give equal weight to all redshifts within the bin. Therefore, the results for a photometric survey would correspond to a very survey-dependent intermediate case between our overlapping and non-overlapping cases. In all cases considered, as in Paper I, we consider $f_{\rm sky} = 1$. It is straightforward to rescale our results for different values of $f_{\rm sky}$.

Finally, we need to set the multipole range that will be used. We explore two different scenarios. First, we consider $\ell \in [2, \ell_{\max}(z)]$ unless otherwise stated, where $\ell_{\max}$ is the multipole corresponding to the smallest scale $k_{\max}$ for which non-linear clustering can be neglected: $\ell_{\max} = k_{\max}\chi(z)$, where $\chi(z)$ is the comoving distance to the mean redshift of the redshift bin of interest. We assume $k_{\max} = R_{\max}^{-1}$, where $R_{\max}$ is the radius of a top-hat window in configuration space for which the variance of the matter fluctuations within a given radius in configuration is unity: $\sigma_{\rm m}(R_{\max}) = 1$. We use $\ell_{\max} = \{180, 550, 1100, 1900, 3000\}$ for $z = \{0.3, 0.7, 1.1, 1.5, 1.9\}$, respectively. In addition, we consider a conservative case in which $\ell_{\max} = 200$ for all redshift bins.

4 Systematic bias induced by different approximations

The results shown in this section aim to be an example of the performance of the methodology described in Section 2, but also to act as a warning for future measurements. For illustration purposes, we choose to apply the methodology to a case where the bias introduced in the best-fit parameters arises only from incorrect modeling. Therefore, in what follows we consider that the only model under study matches the true cosmology, so that $M^{\rm C} = M_0$, while $M^{\rm I}$ refers to the same underlying model but when an incorrect modeling of the observable is used. Furthermore, we take $\boldsymbol{\theta}^{\rm fid,I} = \boldsymbol{\theta}^{\rm fid,C} = \boldsymbol{\theta}_0^{\rm tr}$. This means that the data drawn from M_0 is equal to the prediction for $M^{\rm C}$ using the correct modeling: $C_\ell^{\rm d} \equiv \hat{C}_\ell^{\rm C}(\boldsymbol{\theta}^{\rm fid,C}|M^{\rm C})$. We choose M_0 to be $\Lambda{\rm CDM}+f_{\rm NL}$, with parameter values $\boldsymbol{\theta}_0^{\rm tr}$: $h = 0.6727$, $\omega_{\rm b} = 0.02225$, $\omega_{\rm cdm} = 0.1198$, $n_s = 0.9645$, $f_{\rm NL} = 0$, an amplitude of the primordial power spectrum $\ln 10^{10} A_s = 3.0940$, and we consider three massive degenerate neutrinos with mass $m_\nu = 0.02$ eV each. We assume scale- and redshift-independent Gaussian galaxy bias for the sake of simplicity: $b_G^{\rm unif} = b_G^{\rm Eu-l} = 2$ for the uniform and Euclid-like surveys and $b_G^{\rm SPx} = 1.4$ for the SPHEREx-like survey; this assumption does not change the qualitative results of the examples under study.

The modeling we use to compute $C_\ell^{\rm C}$ and $C_\ell^{\rm d}$ includes relativistic corrections and redshift-space distortions due to peculiar velocities and lensing magnification, and does not use the Limber approximation. In turn, $C_\ell^{\rm I}$ differs from them in one aspect of the modeling: in Section 4.1 $C_\ell^{\rm I}$ does not include the contribution from lensing magnification, while in Section 4.2 $C_\ell^{\rm I}$ uses the Limber approximation. Both cases are explored using a multi-tracer analysis of the angular galaxy power spectra in Section 4.3.

In all cases considered below, the estimated systematic biases correspond to the full vector of the shift in the multidimensional parameter space. Afterwards, we assess the significance of the estimated biases in the marginalized constraints on each of the parameters by

comparing them with the 68% confidence level of their respective marginalized uncertainties, obtained using the same approximations. As a general rule of thumb, the parameter θ_a would be considered significantly biased if the corresponding component of $\boldsymbol{\Delta}_{\text{syst}}$, $\Delta_{\text{syst},a}$, is larger than the 68% confidence level marginalized uncertainty in the inference of θ_a: $\Delta_{\text{syst},a}/\sigma_{\theta_a} \gtrsim 1$. We refer the interested reader to Paper I for a detailed discussion on the effects of approximations on the parameter uncertainties.

4.1 Ignoring lensing magnification

Matter density perturbations along the line of sight affect how we observe the galaxy density distribution [64]. Therefore, the observed galaxy number count perturbations are determined by the intrinsic clustering, redshift-space distortions due to peculiar velocities and relativistic corrections. These corrections can be separated into contributions from lensing magnification, doppler, and gravitational potential effects such as time-delays and integrated Sachs-Wolfe effect [65–70].

Lensing magnification is a subdominant contribution to the observed galaxy overdensities except when the redshift separation between bins is large enough so that the correlation due to intrinsic clustering is negligible. However, it is normally the largest relativistic correction, especially when cross-correlating two different redshift bins using the angular power spectrum [71]. Some arguments against including lensing magnification include its subdominant relative contribution to the galaxy power spectrum at the scales explored so far, the large computational expenses required for its calculation and the difficulties in obtaining an accurate determination of the magnification bias parameter (see e.g., [72]). Nonetheless, the magnification contribution contains cosmological information complementary to weak-lensing shear [25, 73, 74].

To understand and model the effect of lensing magnification consider that the gravitational lensing contribution to the galaxy overdensity consists of two competing effects: on the one hand, it stretches the volume behind the lens; on the other, it magnifies individual sources and promotes faint galaxies above the magnitude limit of the survey [75]. This changes the observed galaxy number density n_{obs} in a flux-limited survey:

$$n_{\text{obs}} = n\left[1 + (5s - 2)\kappa\right], \tag{4.1}$$

where n is the intrinsic galaxy number density, s is the magnification bias parameter, and κ is the convergence [76]. Note that $s = 0.4$ corresponds to a vanishing contribution from lensing magnification. Since the magnification bias parameter depends on the tracer used, we distinguish between s^X and s^Y. We do not consider s as a nuisance parameter (as should be done in a more quantitative analysis of actual observations); instead, we study several cases with different constant values of s in order to study the dependence of the systematic biases on this parameter.

We show the significance of the estimated biases when lensing magnification is neglected as a function of the magnification bias parameter in Figure 1. Considering only single-tracer analyses, we show results for the uniform and Euclid-like galaxy surveys, and normalize the estimated biases with the forecasted 68% confidence level marginalized constraints in order to show the bias significance. We find that the size of the systematic bias grows as $|s - 0.4|$ increases, and that it grows faster for magnified populations (i.e., $s > 0.4$), than for demagnified. Results for different redshift distributions are qualitatively very similar. The only difference is that, for $\ell_{\text{max}} = 200$, the estimated biases are larger for the uniform survey than for the Euclid-like survey when the redshift bins overlap, and viceversa when the redshift
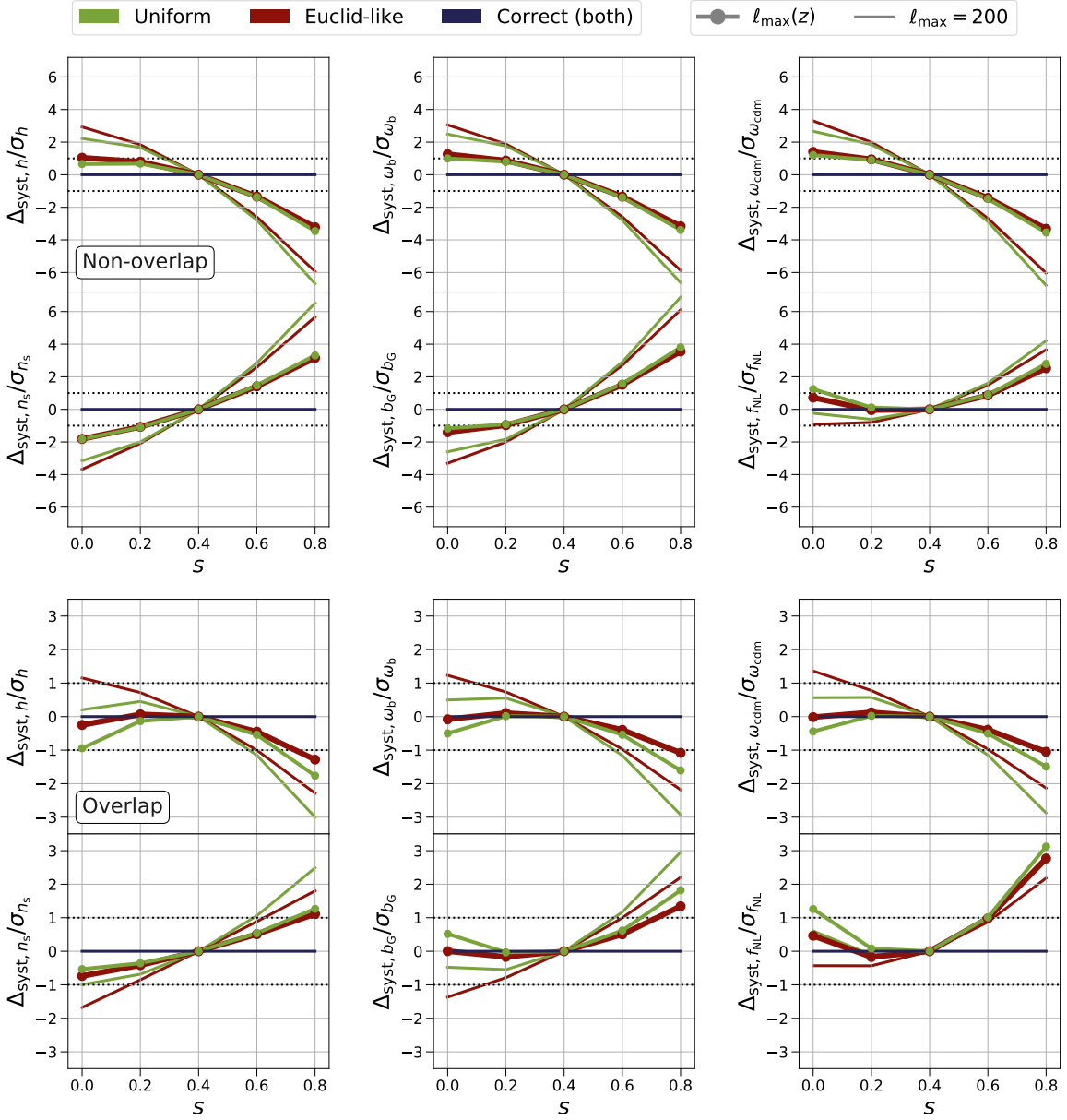
Figure 1: Ratio of the estimated bias in the model parameters over the forecasted 68% confidence level marginalized constraints for cases when the lensing magnification is included (blue) and not as a function of the assumed magnification bias parameter. We show results for uniform (green) and Euclid-like (red) galaxy redshift distributions, and with non-overlapping (top) and overlapping (bottom) redshift bins; note the change of scale in the y-axis between them. In all cases, the case for $\ell_{\mathrm{max}}(z)$ is shown with wide solid lines with circle markers, while thin solid lines without markers correspond to the case with constant $\ell_{\mathrm{max}} = 200$. Dotted lines mark $|\Delta_{\mathrm{syst},a}/\sigma_{\theta_a}| = 1$.

bins do not overlap. While for the Euclid-like survey the biases are always larger when the redshift bin do not overlap, this is only true for the uniform survey when $s > 0.4$.

In general, the significance of the bias is much larger for the case in which $\ell_{\mathrm{max}} = 200$

than when ℓ_{max} varies with redshift (reaching higher values). This may be counter-intuitive, since the signal-to-noise ratio of the magnification contribution increases at smaller scales. However, the higher-ℓ part is computed only for the highest-z bins (see Section 3.1), so that the relative contribution of lensing magnification is smaller at these scales (remember that lensing magnification dominates the angular power spectra for very separated redshift bins). Moreover, the constraints on the cosmological parameters also improve for increasing ℓ_{max}, and $\Delta\boldsymbol{\theta} \propto F^{-1}$. The reduction of the significance of the bias with higher ℓ_{max} can be understood as the information beyond lensing magnification encoded in the angular galaxy power spectra having more weight in the final parameters constraints, with respect to the $\ell_{\mathrm{max}} = 200$ case.

Assessing the significance of the biases exploring only one-dimensional marginalized parameter constraints might be misleading. The bias might be much more significant for systematic shifts in perpendicular directions to parameter degeneracies than what would be inferred from one-dimensional projections. We show forecasted two-dimensional marginalized constraints for all parameter combinations from a single-tracer Euclid-like survey in the $\ell_{\mathrm{max}}(z)$ case including the estimated biases with respect to the fiducial cosmology in Figure 2. We compare the case including magnification (with $s = 0.8$) and the case without including magnification (shown in blue and red, respectively). We show results for the non-overlap (overlap) redshift bin configuration in dark (light) colors. As found in Paper I, the parameter degeneracies obtained neglecting lensing magnification are not necessarily the same as for the correct analysis. Furthermore, we find the systematic bias to be aligned with the degeneracies of the incorrectly estimated constraints. Whether the alignment is general or depends on the observable is beyond the scope of this work. As expected from Figure 1, the biases shown in Figure 2 are larger for the case with non-overlapping redshift bins. Finally, while the correct uncertainties do not depend on whether the redshift bins overlap or not, the resulting incorrect confidence level regions (i.e., neglecting magnification) are slightly larger when the redshift bins overlap (which further reduces the significance of the bias). The results using $\ell_{\mathrm{max}} = 200$ are qualitatively similar (with a higher significance of the bias, as shown in Figure 1).

4.2   Using the Limber approximation

As shown in Equation (3.2), the angular power spectrum is the projection along the line-of-sight of the spatial, three-dimensional power spectrum. The transfer functions that drive this projection include spherical Bessel functions. Therefore, integration over two spherical Bessel functions is needed to compute C_ℓ for each multipole. Given the oscillatory nature of the spherical Bessel functions, it is very computationally expensive to ensure the convergence of these integrals, which slows down the calculation of C_ℓ. The Limber approximation [77–79] aims to alleviate this problem by approximating the spherical Bessel functions as Dirac delta functions. However, the transformation of low-order spherical Bessel functions (i.e., low ℓ) into Dirac delta functions is not accurate, which means that the Limber approximation breaks down for C_ℓ at large scales. Using the Limber approximation to compute the galaxy power spectrum may introduce significant biases in cosmological parameters, even when combined with galaxy weak lensing observations, for which the Limber approximation is accurate enough (see e.g. [80]).

We show two-dimensional forecasted marginalized constraints on the cosmological parameters from the angular power spectrum of a single-tracer Euclid-like galaxy survey in Figure 3. We show results using $\ell_{\mathrm{max}}(z)$ both with and without the Limber approximation
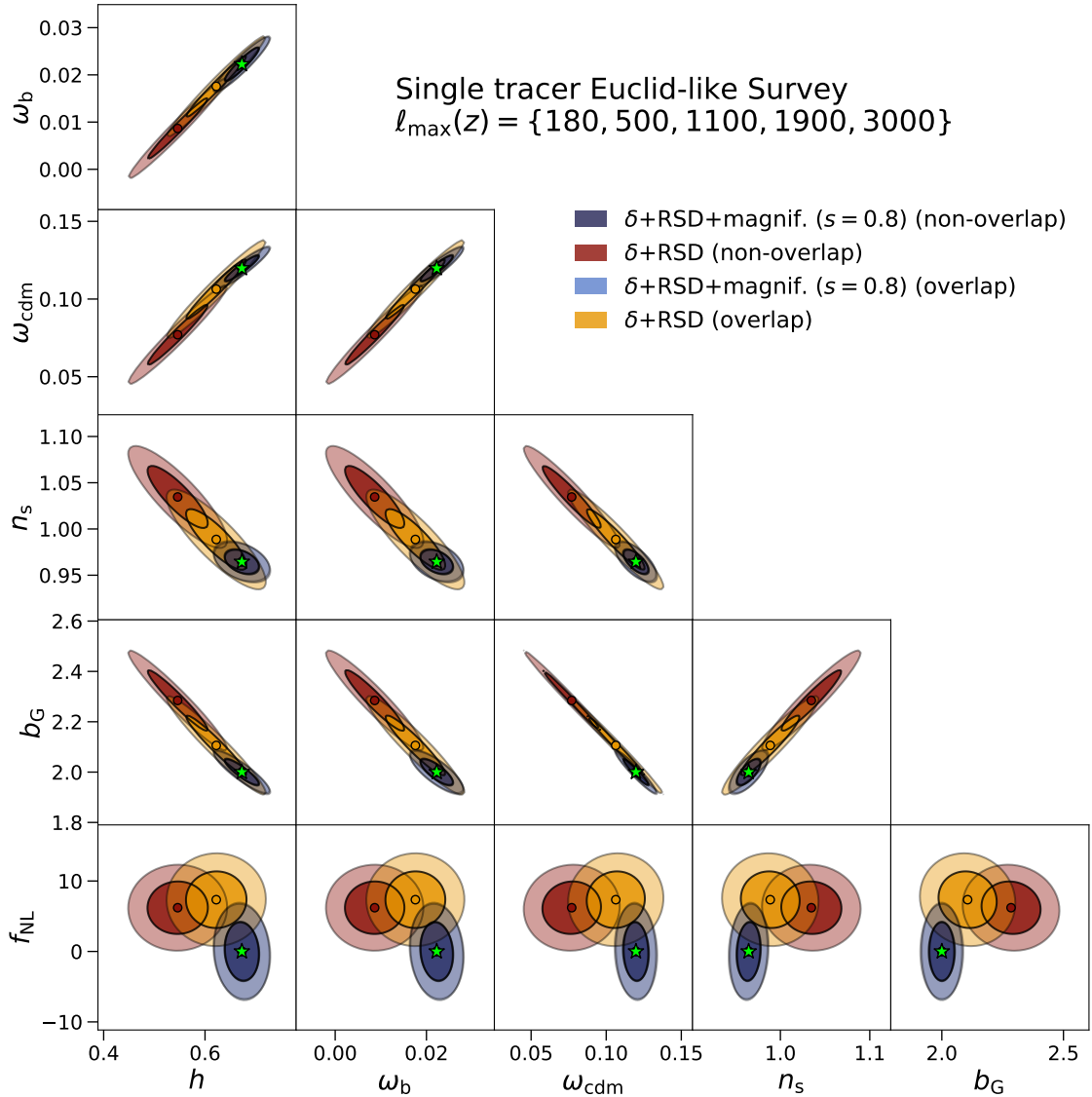
Figure 2: 68% and 95% confidence level estimated marginalized constraints on the model parameters for a Euclid-like survey with a single tracer with $s = 0.8$ using $\ell_{\max}(z)$. We compare the results including cosmic magnification (blue) and without including it (red), assuming that the fiducial cosmology assumed coincides with the actual one, marked with a star. Dark colors (blue and red) refer to the case with non-overlapping redshift bins, while light colors (light blue, orange), refer to the case with overlapping redshift bins.

(red and blue, respectively), and show the results with overlapping redshift bins in lighter colors. We assume $s = 0.4$ in order to avoid contributions from lensing magnification. As noted in Paper I, parameter uncertainties are underestimated when the Limber approximation is used, especially for non-overlapping redshift bins. This makes the (generally) small shifts in the best-fit values more significant when compared to the small forecasted errors. The bias is especially worrisome for f_{NL}, the only example where the shift in the best fit is very large.
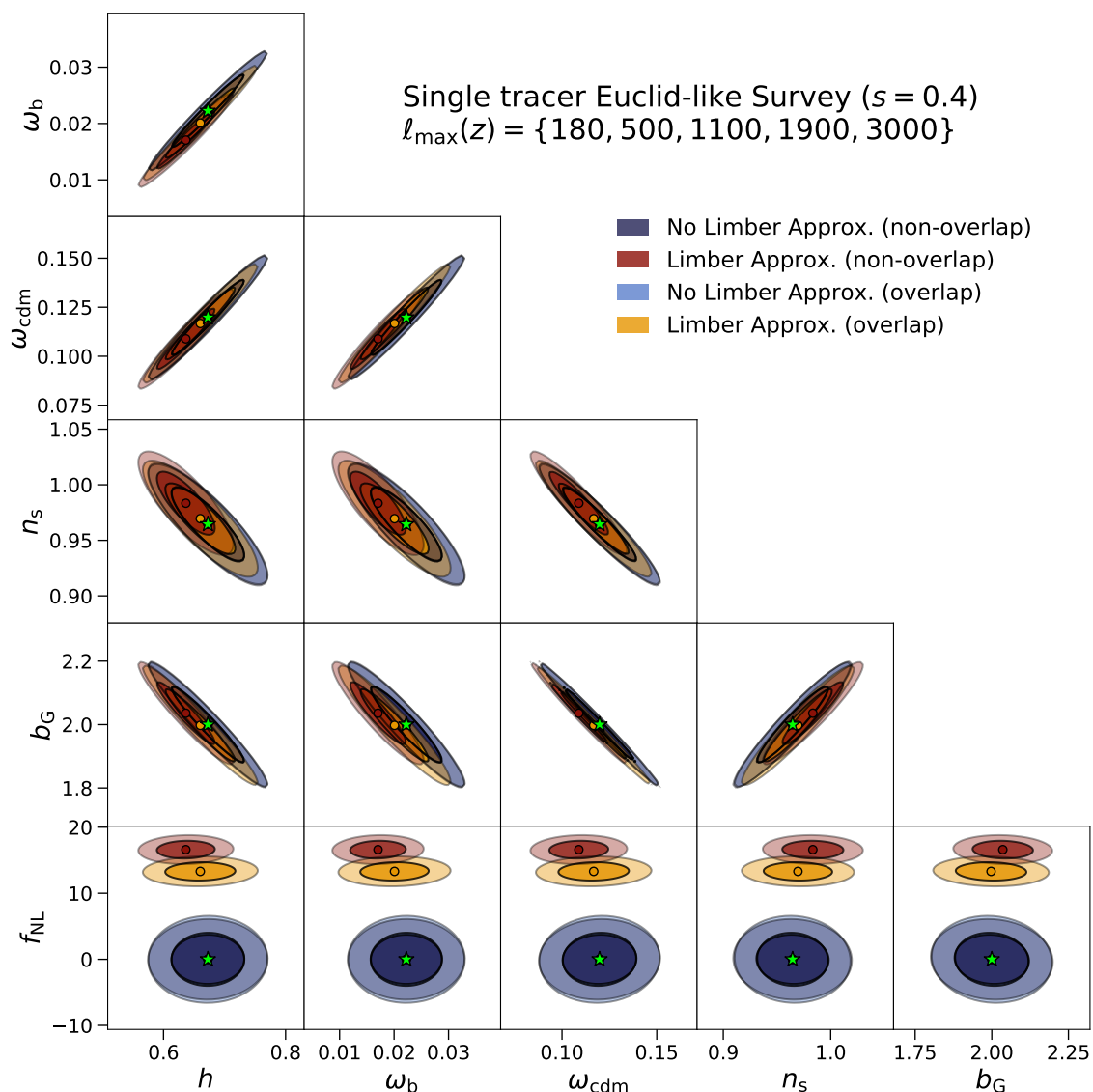
Figure 3: Same as Figure 2, but comparing the results with and without using the Limber approximation and assuming $s = 0.4$.

This is because the signature of local primordial non-Gaussianities manifests at large scales, which is where the Limber approximation breaks down. The estimated systematic bias in f_{NL} is $\gtrsim 18(14)\sigma$ for the case with non-overlapping (overlapping) redshift bins. This result indicates that using the Limber approximation at large scales potentially leads to a false positive detection of primordial non-Gaussianity. In general, biases are smaller when the redshift bins overlap, as it was the case for the non-inclusion of lensing magnification of the signal. The results using $\ell_{\max} = 200$ are qualitatively similar, with the weaker constraints (due to the use of a narrower multipole range) but with a comparable significance of the bias due to the use of the Limber approximation. This is because the Limber approximation breaks down at low ℓ, which is a regime covered in both cases.

4.3 Multi-tracer galaxy power spectrum

One of the most exciting prospects offered by the next-generation galaxy surveys is the possibility to perform multi-tracer analyses [81, 82]. Instead of using all galaxies as a single tracer, using various tracers of the underlying density field at the same time and fully accounting for their cross-correlations, provides additional information. The gain comes from probing the same volume more than once, each time with a different galaxy bias, which reduces the cosmic variance for quantities that are related to the galaxy bias. Besides tightening the constraints on all cosmological parameters, especially those related with the galaxy bias, the use of multi-tracer approaches are expected to be especially effective to constrain physics that affect the large scales, such as local primordial non-Gaussianities.

Given the reduced cosmic variance, systematic errors may produce more significant biases in parameter inference than for single-tracer studies. We apply the methodology described in Section 2 to multi-tracer analyses of the angular galaxy clustering in order to asses the impact of the approximations discussed above. We use Multi_CLASS to compute the angular cross-power spectrum of two different tracers (with their own redshift distribution, galaxy bias and magnification bias parameter). We consider two different galaxy surveys (or galaxy populations observed by the same survey) following a Euclid-like and a SPHEREx-like redshift distribution and with different galaxy bias as specified in Section 3.1.

We show forecasted two-dimensional marginalized constraints of the cosmological parameters under study with and without modeling lensing magnification and using $\ell_{\max}(z)$ in the signal and covariance in Figure 4. For illustrative purposes, we focus just on the case with magnification bias parameters $s^{\mathrm{Eu-l}} = s^{\mathrm{SP-l}} = 0.6$ for the Euclid-like and SPHEREx-like surveys. The figure also includes the estimated bias in the best-fit parameters. We can appreciate that, as reported in Paper I, ignoring lensing magnification overestimates the uncertainties in the parameters, except for f_{NL} (and ω_{b}, for which there is practically no effect). Moreover, there are still significant biases ($\sim 1 - 2\sigma$) in all parameters when the redshift bins do not overlap (shown in darker colors). Surprisingly, the systematic bias is much less significant ($\lesssim 1\sigma$) when the redshift bins do overlap. As in Figure 2, the estimated bias is aligned with the degeneracy between the parameters, which almost does not change whether lensing magnification is included or not. The alignment between the bias and the parameter degeneracies is most likely not generic, but very population selection (and thus, survey) dependent. With a slightly different set up (or different fiducial s for the two populations) this alignment may not hold. Such scenario may lead to great impact in final results: a change in the degeneracies would greatly exacerbate the effect of the systematic bias introduced by approximations when combining the angular galaxy power spectra with other cosmological probes.

Similarly to the single-tracer case, the estimated bias found when using $\ell_{\max} = 200$ is larger than using $\ell_{\max}(z)$, but the degeneracies and direction of the shifts remain unchanged. The increase of the significance of the bias using $\ell_{\max} = 200$ instead of $\ell_{\max}(z)$ is smaller than for the single-tracer case. This is because the multi-tracer approach reduces the cosmic variance, so that the relative contribution to the constraints from large scales in the $\ell_{\max}(z)$ case is higher than in the single-tracer case and the effect of using $\ell_{\max} = 200$ is smaller.

Figure 5 shows the analogous results for using or not the Limber approximation (and considering lensing magnification in both cases). The uncertainties of the parameters are underestimated at approximately the same level as for the single-tracer case, but the estimated biases are larger in this case. Note also that in some cases the biases is not aligned with the parameter degeneracies. As for the Euclid-like only analysis shown in the previous
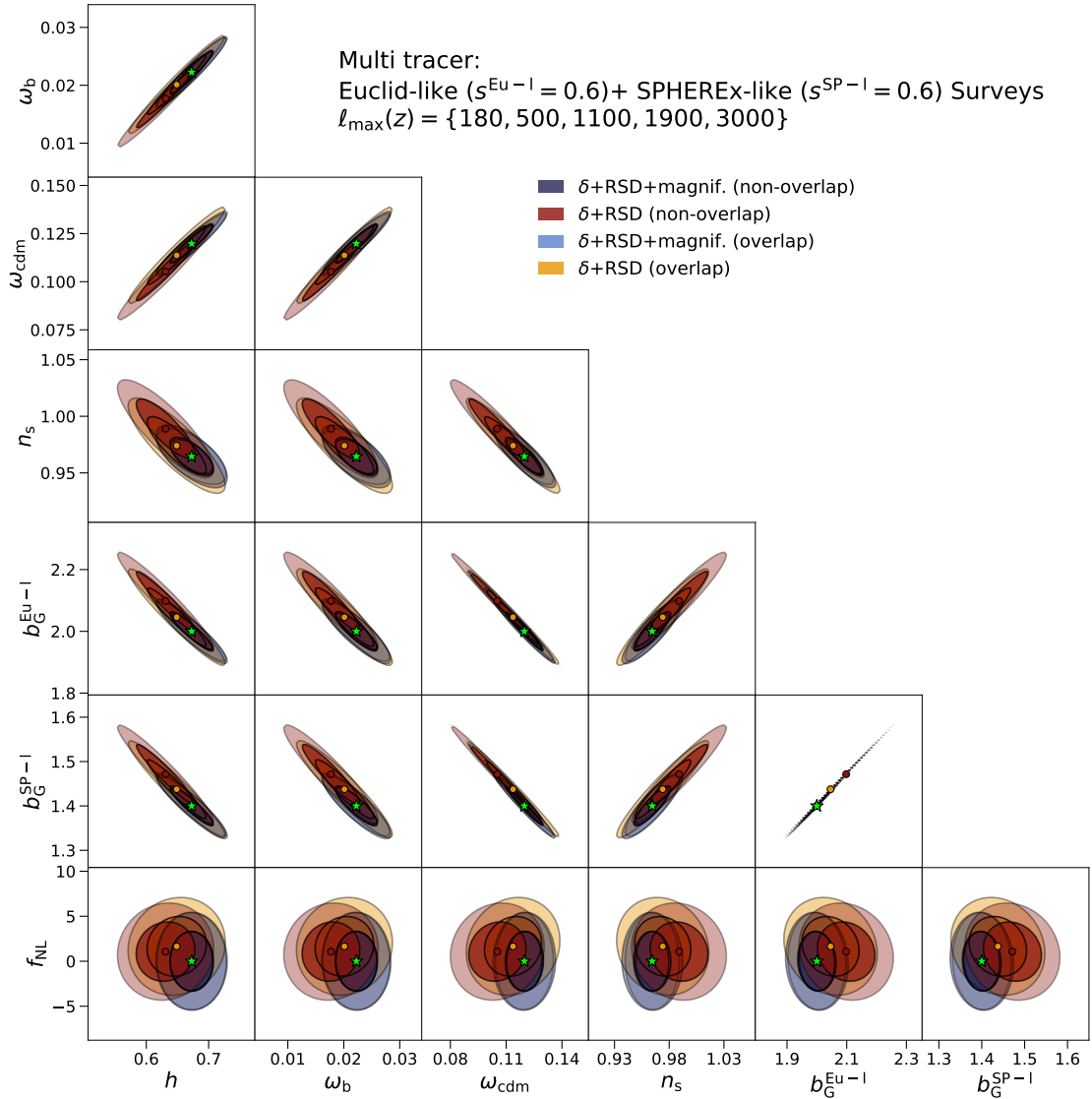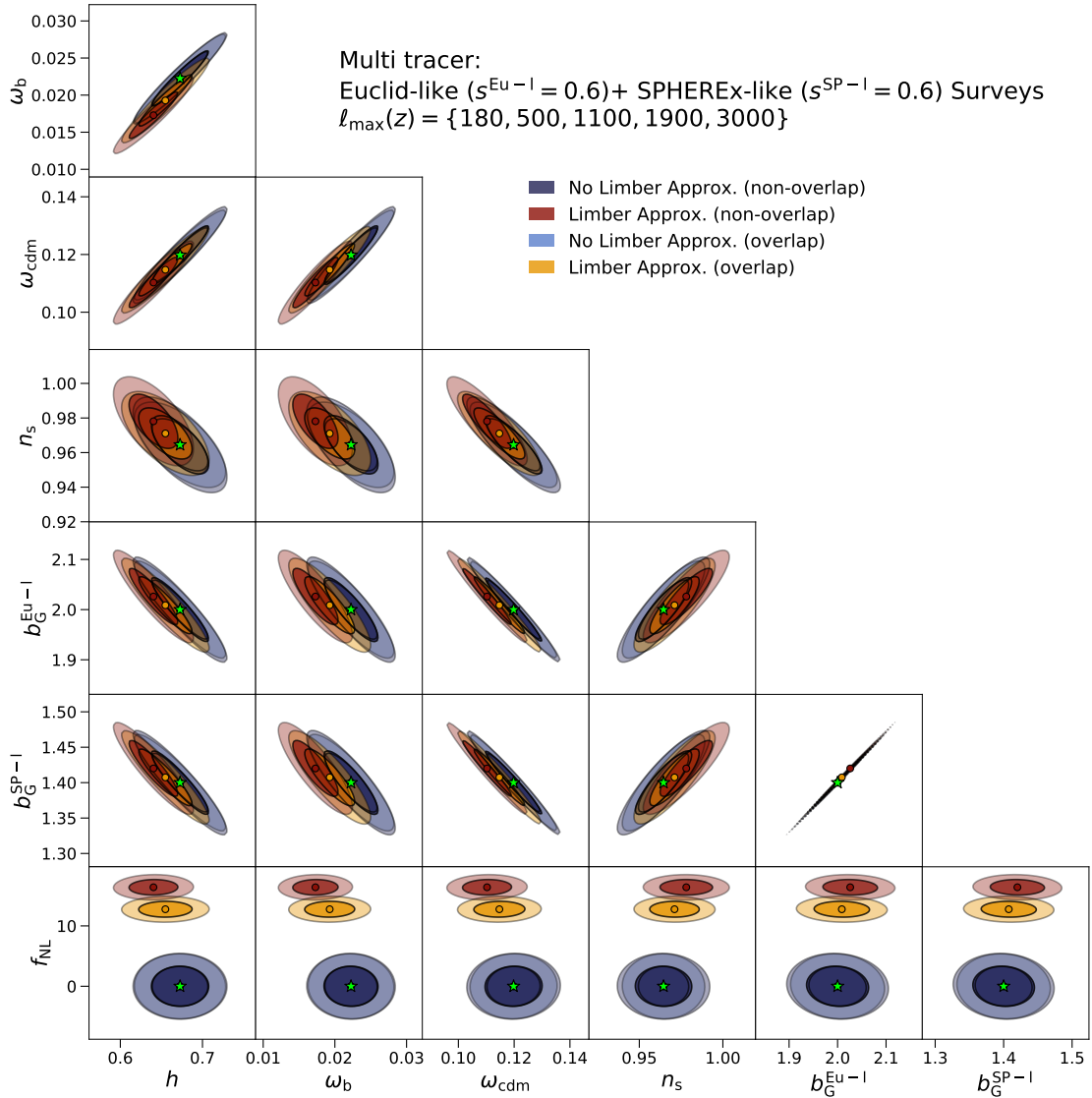
Figure 4: Same as Figure 2, but for a multi-tracer analysis of the Euclid-like and SPHEREx-like surveys considered in this work, assuming $s = 0.6$ for both surveys.

section, the biases are smaller for overlapping bins (lighter colors) than for non-overlapping bins, because when the redshift bins overlap biases are smaller and incorrect uncertainties are larger. In this case f_{NL} is again by far the most affected parameter, with biases of $19\sigma\,(14\sigma)$ for non-overlapping (overlapping) redshift bins. In this case, as for the single-tracer case, the results using $\ell_{max} = 200$ are very similar to those shown in Figure 5.

Finally, we can compare the estimated marginalized biases for the Euclid-like only analyses and for the multi-tracer analysis combining the Euclid-like and the SPHERE-like surveys. We show the ratio of the estimated biases over the forecasted 68% confidence level marginalized constraints for both cases (using both $\ell_{max}(z)$ and $\ell_{max} = 200$) in Figure 6. We show results both for overlapping and non-overlapping bins, and using separately the two approxi-

Figure 5: Same as Figure 3, but for a multi-tracer analysis of the Euclid-like and SPHEREx-like surveys considered in this work, assuming $s = 0.6$ for both surveys.

mations considered in this work: neglecting lensing magnification (left panel), and using the Limber approximation (right panel). Figure 6 shows in clearer way the comparison between the single-tracer and multi-tracer cases and using different criteria for ℓ_{max} discussed above. When lensing magnification is not included the biases are approximately the same for both single- and multi-tracer analyses if $\ell_{max}(z)$, while they are larger for a single-tracer analysis if $\ell_{max} = 200$. In all cases, the estimated biases are larger for non-overlapping redshift bins. Regarding the use of the Limber approximation, the biases are larger for all parameters for the multi-tracer case. The dependence of the estimated biases on the criterion used for ℓ_{max} is not significant, except for ω_b and f_{NL}. Finally, the estimated biases are again always larger for the non-overlapping redshift bins, with a special mention to f_{NL}, the difference of which
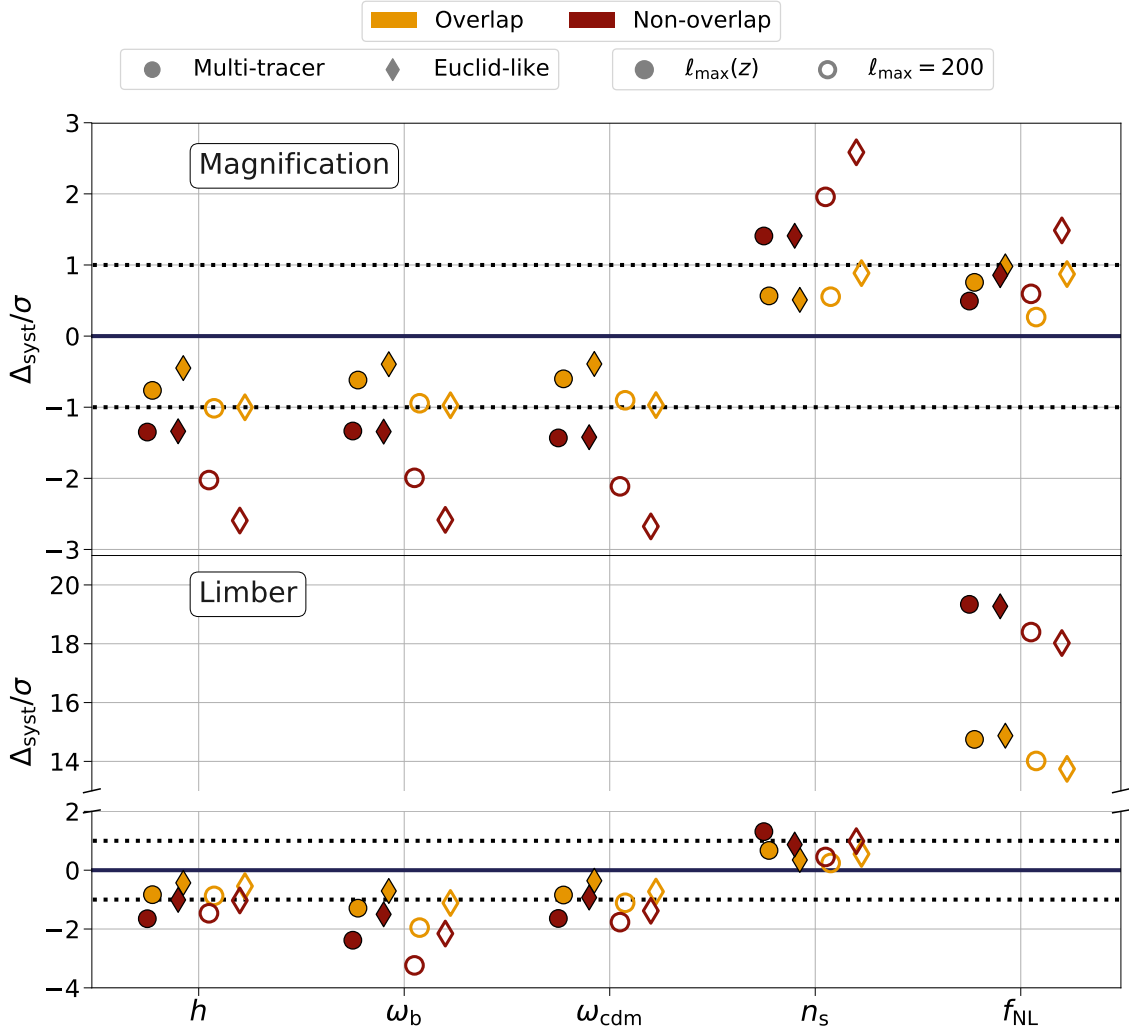
Figure 6: Ratio of the estimated bias in the cosmological parameters over the forecasted 68% confidence level marginalized constraints for cases when the lensing magnification is not modeled (upper panel) and the Limber approximation is used (bottom panel). We show results considering an Euclid-like survey (diamonds), and its combination with a SPHEREx-like survey performing a multi-tracer analysis (circles), both for overlapping (orange) and non-overlapping (red) redshift bins. In all cases we consider $s = 0.6$ for both galaxy populations. Filled (hollow) markers refer to results using $\ell_{max}(z)$ ($\ell_{max} = 200$), respectively. Note the different scale in the y-axis in each panel, and that the y-axis in the right panel is broken. Dotted lines mark $|\Delta_{syst,a}/\sigma_{\theta_a}| = 1$.

is more than 4σ.

Although exploiting higher multipoles of the angular galaxy power spectra returns smaller biases for the specific sources of theoretical systematic errors explored in this work, we emphasize that there are other key features in the modeling of the observable susceptible to induce a bias in the best-fit parameters. The modeling of non-linear clustering is probably the most important one, and it arises at small scales. Therefore, we advocate for a comprehensive estimation of potential biases in the inferred best-fit parameters using the

methodology described in this work, accounting for all possible sources of systematics or approximations adopted, before freezing the analysis pipeline.

5 Conclusions

Cosmology needs to transition from the precision to the accuracy era. Reducing the systematic error budget below the statistical uncertainties represents a crucial step in that direction. Besides controlling observational systematics, improved theoretical models of cosmological observables will be needed. Approximations that have been accurate enough so far, may introduce significant systematic errors for forthcoming experiments.

There are two kind of errors that can be introduced into an analysis: a modification of the shape of the posterior distribution and a shift of the location of its peak. These produce a misestimation of the model parameters covariance and a systematic bias on their best-fit values. While the former has been studied on a companion paper [44], here we have focused on the latter.

Expanding upon previous works, we have completely generalized the methodology to estimate the systematic bias introduced in parameter inference when the theoretical model for a given measurement is not accurate enough or the assumed underlying model is not incorrect. The generalized methodology is equally applicable to any measurement, even beyond the field of cosmology. Given the complete flexibility and easy to use of Equations (2.5) and (2.7) , we advocate their implementation whenever different approximations are under consideration.

This methodology can also be useful to optimize analyses that rely on an assumed fiducial cosmology. Since this may introduce a systematic bias (see e.g., [83] for a detailed study in the case of the BAO analysis), our methodology can be iteratively applied to find a fiducial cosmology with a prediction more concordant with the measurements. The methodology used in this work assumes Gaussian posteriors since it is based on the Fisher matrix formalism, but this assumption can be relaxed, following [84–87]. This assumption is also dropped when expanding the observable up to higher order on the model parameters. We derive the estimation of the bias when doing a second order expansion in Appendix A.

To show the performance of the generalized methodology, we have applied it to the angular galaxy power spectra as observed by next generation galaxy surveys. Instead of considering specific examples, we have used straw-man, yet realistic, galaxy-survey specifications and have shown how neglecting lensing magnification or using the Limber approximation can bias cosmological parameter inference. We have found significant biases (most of them $\gtrsim 1\sigma$) in all the cases explored in this work. Moreover, we have also included examples of multi-tracer analyses, using Multi_CLASS, a modified version of CLASS which allows to compute the angular cross-power spectra for two different tracers of the matter distribution. In general, we have found that the estimated systematic biases due to the considered approximations are more significant for multi-tracer analyses.

We stress that our results cannot be taken quantitatively at face value because the significance of the biases are expected to be very dependent on the survey and galaxy population specifications. Nonetheless, the risk of introducing significant systematic biases in the results is general, and our work must be considered as a warning for analyses of future experiments. Although, for illustration, we have focused in just two sources of theoretical systematic errors, there are many other potential origins of systematic errors, both observational and theoretical. Therefore, it is of crucial importance that any source of systematics is reduced well below the 1σ statistical uncertainty to ensure the robustness of the results. This

is because the joint contribution of small systematic errors can significantly bias the inferred constraints otherwise, even if the sources of systematics are unrelated between them.

Considering the dramatic experimental upgrades that many fields of physics will experience in the coming years, it is of paramount importance to fully exploit the potential of new experiments and to obtain unbiased results. To do so, we need to estimate potential biases introduced by approximations under consideration. In this work, we have provided a methodology to do that and estimate the significance of systematic biases introduced in parameter inference. Finally, we envision that our generalized methodology will also be useful to single out possible sources of systematic errors affecting new or unexpected findings.

Acknowledgments

A   Evaluation of the estimation of the systematic shift and higher order approximations

In Section 2, we have presented a general expression to estimate systematic shifts on the best-fit parameters due to incorrect modeling. Equation (2.5) is obtained assuming a Gaussian likelihood and expanding the response of the observables to small variations in the model parameters up to linear order. In this appendix we evaluate the performance of this approximation, and extend the discussion of Section 2 considering the expansion up to second order and for a common non-Gaussian likelihood corresponding to variables following a Wishart distribution.

A.1   Accuracy of the estimation

According to the Fisher forecast approach, the results for the systematic shift on the best-fit parameters shown in the main text rely on a linear expansion of the observable on the model parameters (see Equation (2.2)). However, this expansion is not accurate for large displacements $\Delta\theta$ in parameter space, unless the observable is linear on the model parameters. Moreover, the approach intrinsically assumes a Gaussian posterior.

Here we compare the shift on the best-fit parameters estimated in that way to those found from a numerical evaluation of the Gaussian likelihood for the angular galaxy power spectrum. For the sake of simplicity and clarity, we consider a simplified case, in which the only free parameters are $n_{\rm s}$ and $f_{\rm NL}$, and all other parameters are kept fixed. We focus on the bias introduced by ignoring the contribution of lensing magnification for an Euclid-like survey with overlapping redshift bins, $\ell_{\max} = 200$, and representative fiducial values for the magnification bias parameter $s = \{0.4, 0.6, 0.8\}$. We generate mock data (i.e. angular
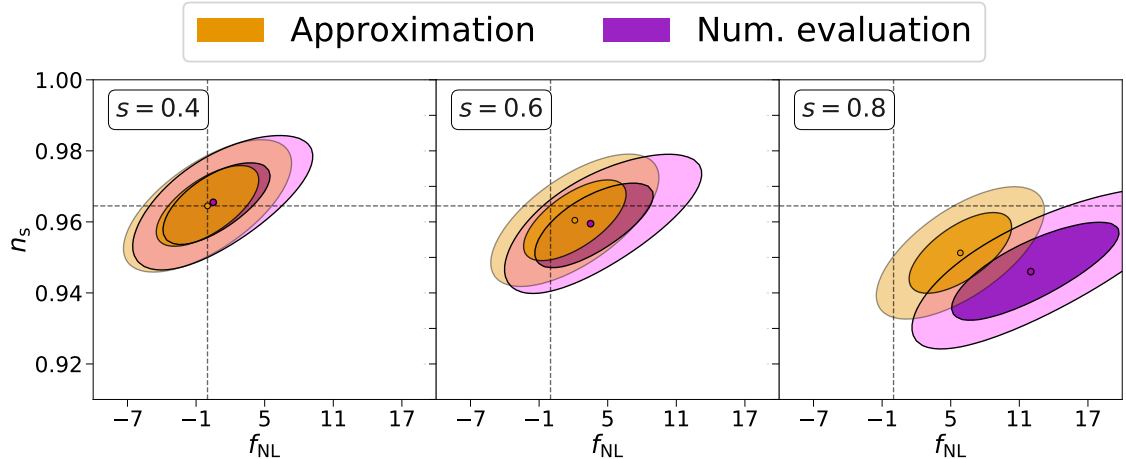
Figure 7: Estimated and numerically evaluated shifts induced by neglecting lensing magnification with $s = 0.4$, 0.6 and 0.8 (left, middle and right panel, respectively). Comparison of the forecasted constraints and estimated bias in the best-fit values using the formalism explained in Section 2 (orange) to the results obtained by a numerical evaluation of the likelihood (pink). We show 68% and 95% confidence level constraints for an Euclid-like survey and using $\ell_{\max} = 200$ for all redshift bins. Dashed grey lines mark the values used to compute the mock data. In the left panel the small discrepancy in the best-fit values is due to the discrete grid adopted in the numeric evaluation.

power spectra) assuming the fiducial cosmology and including lensing magnification. We do not include sample variance in the mock data, to ease the comparison. We compute the likelihood of the angular galaxy power spectra for values of f_{NL} and n_{s} in a two-dimensional grid, without including lensing magnification (i.e., assuming $s = 0.4$).

The comparison is shown in Figure 7. This figure demonstrates that the estimate of Equation (2.5) (Equation (3.6) for this specific case) and the formalism discussed in Section 2 are qualitatively correct. However, as expected, the accuracy of the estimate decreases as the modelling error (and hence the bias introduced in the best-fit parameters) increases. In this case, our approach with a linear-order expansion underestimates the bias on the model parameters. Nonetheless, this is very likely to be very case-dependent. For the relevant cases where the bias in the parameter inference is small, the linear approximation provides a good estimates. For other cases, it is possible to use a second order approximation, as explained below.

It is however important to note that, in general, if the simple estimate (2.5) predicts a negligile shift, it is safe to adopt the approximation considered. On the other hand, if the simple estimate (2.5) predicts a large shift, even if the shift amplitude is not estimated precisely, it is still a clear indication that the approximation considered should not be adopted.

A.2 Systematic shift using a second order expansion

Let us consider a second order expansion of the response of the observable Ψ to a variations of the model parameters around their fidicual values $\boldsymbol{\theta}^{\mathrm{fid}}$:

$$\hat{\Psi}_i(\boldsymbol{\theta}^{\mathrm{fid}} + \Delta\boldsymbol{\theta}) \approx \hat{\Psi}_i^{\mathrm{fid}} + \left(\boldsymbol{\nabla}_\theta \hat{\Psi}_i^{\mathrm{fid}}\right)^T \Delta\boldsymbol{\theta} + \frac{1}{2}\Delta\boldsymbol{\theta}^T \left(\mathcal{H}_\theta \hat{\Psi}_i^{\mathrm{fid}}\right) \Delta\boldsymbol{\theta}, \tag{A.1}$$

where $\mathcal{H}_\theta$ is the Hessian operator (with derivatives with respect to the model parameters), applied to the observable $\hat{\Psi}_i$ and evaluated at $\boldsymbol{\theta}^{\mathrm{fid}}$. This expansion adds the last term to the linear expansion shown in Equation (2.2). Now we can proceed as explained in Section 2: if we substitute this expansion in the logarithm of the likelihood (Equation (2.1)) and maximize it, we find

$$\sum_{i,j} \left[\boldsymbol{\nabla}_\theta \hat{\Psi}_i^{\mathrm{fid}} + \left(\mathcal{H}_\theta \hat{\Psi}_i^{\mathrm{fid}} \right) \Delta\boldsymbol{\theta} \right] \left(\mathrm{Cov}^{-1} \right)_{ij}$$
$$\left[\Psi_j^{\mathrm{d}} - \hat{\Psi}_j^{\mathrm{fid}} - \left(\boldsymbol{\nabla}_\theta \hat{\Psi}_j^{\mathrm{fid}} \right)^T \Delta\boldsymbol{\theta} - \frac{1}{2} \Delta\boldsymbol{\theta}^T \left(\mathcal{H}_\theta \hat{\Psi}_j^{\mathrm{fid}} \right) \Delta\boldsymbol{\theta} \right] = 0 \,. \tag{A.2}$$

After some algebra we can simplify this expression to

$$\sum_{i,j} \left(\boldsymbol{\nabla}_\theta \hat{\Psi}_i^{\mathrm{fid}} \right) \left(\mathrm{Cov}^{-1} \right)_{ij} \left(\Delta\hat{\Psi}_j^{\mathrm{fid}} \right) = F\Delta\boldsymbol{\theta} - \sum_{i,j} \left(\mathcal{H}_\theta \hat{\Psi}_i^{\mathrm{fid}} \right) \Delta\boldsymbol{\theta} \left(\mathrm{Cov}^{-1} \right)_{ij} \Delta\hat{\Psi}_j^{\mathrm{fid}} +$$
$$+ \sum_{i,j} \left[\left(\mathcal{H}_\theta \hat{\Psi}_i^{\mathrm{fid}} \right) \Delta\boldsymbol{\theta} \left(\mathrm{Cov}^{-1} \right)_{ij} \left(\boldsymbol{\nabla}_\theta \hat{\Psi}_j^{\mathrm{fid}} \right)^T + $$
$$+ \frac{1}{2} \left(\boldsymbol{\nabla}_\theta \hat{\Psi}_i^{\mathrm{fid}} \right) \left(\mathrm{Cov}^{-1} \right)_{ij} \Delta\boldsymbol{\theta}^T \left(\mathcal{H}_\theta \hat{\Psi}_j^{\mathrm{fid}} \right) \right] \Delta\boldsymbol{\theta} +$$
$$+ \sum_{i,j} \left[\frac{1}{2} \left(\mathcal{H}_\theta \hat{\Psi}_i^{\mathrm{fid}} \right) \Delta\boldsymbol{\theta} \left(\mathrm{Cov}^{-1} \right)_{ij} \Delta\boldsymbol{\theta}^T \left(\mathcal{H}_\theta \hat{\Psi}_j^{\mathrm{fid}} \right) \Delta\boldsymbol{\theta} \right] \tag{A.3}$$

where each line in the right hand side of the expression corresponds to terms linear, quadratic and cubic on $\Delta\boldsymbol{\theta}$, respectively, and we define the difference between the data and the prediction at $\boldsymbol{\theta}^{\mathrm{fid}}$ as $\Delta\hat{\Psi}^{\mathrm{fid}} \equiv \Psi^{\mathrm{d}} - \hat{\Psi}^{\mathrm{fid}}$. Equation (A.3) does not have an analytic solution (which instead exists for a linear expansion, see Equation (2.5)), but can be used if a more accurate estimate is needed, as it may be the case for large $\Delta\boldsymbol{\theta}$. Note that the presence of $\mathcal{H}_\theta$ involves further computation of second derivatives. Finally, Equation (A.3) can be manipulated as described in Section 2 in order to consider the combination of likelihoods.

A.3 Shift for a non-Gaussian likelihood: Wishart distribution

Although the procedure followed in Section 2 to estimate the systematic bias introduced in the best-fit parameters is general for any likelihood, the results given in Equations (2.5) and (A.3) assume a Gaussian likelihood. While in many applications the adoption of a Gaussian likelihood is well justified, this is not always the case. Given that the actual expression for $\Delta\boldsymbol{\theta}$ can differ depending on the likelihood, it is important to explore non-Gaussian cases.

As discussed in Paper I, using a Gaussian likelihood for the angular galaxy power spectra is an approximation based on the central limit theorem: the true Gaussian[6] random variables are the spherical harmonics coefficients associated to the galaxy number density perturbations. Hence, the angular power spectra follow a Wishart distribution. Since we have used the angular galaxy power spectra in this work, here we derive $\Delta\boldsymbol{\theta}$ for a likelihood of variables following a Wishart distribution.

Let us consider a Gaussian variable φ (e.g., the galaxy number density fluctuations), the covariance of which is given by the quantity Φ, considered Gaussian throughout this work,

---

[6]Non-linear clustering induces small deviations from Gaussianity, but these are significant only at small (i.e., non-linear) scales.

but actually following a Wishart distribution. In most of the real cases analogous to this situation, φ is given by the data, and the dependence on the model is encoded in $\hat{\Phi}$. Ψ (i.e., the observable considered in Section 2) is the half-vectorization of Φ; this is analogous to $\boldsymbol{C}_\ell$ and $\mathcal{C}_\ell$, discussed in Section 3. If we consider a Gaussian likelihood for φ, neglecting constant terms, we have

$$
\begin{aligned}
-2\log\mathcal{L}\left(\varphi^{\mathrm{d}}|M,\boldsymbol{\theta}\right) &= \sum_{i,j}\varphi_i^{\mathrm{d}}\left(\hat{\Phi}^{-1}(\boldsymbol{\theta})\right)_{ij}\left(\varphi_j^{\mathrm{d}}\right)^* + \log\left|\hat{\Phi}(\boldsymbol{\theta})\right| = \\
&= \sum_{p,q}\left[\Phi_{pq}^{\mathrm{d}}\left(\hat{\Phi}^{-1}(\boldsymbol{\theta})\right)_{qp}\right] + \log\left|\hat{\Phi}(\boldsymbol{\theta})\right|,
\end{aligned}
\tag{A.4}
$$

where the last equality yields the likelihood for Φ^{d}, following a Wishart distribution with the parameter dependence encoded in the matrix $\hat{\Phi}$. The maximization condition for this likelihood is (dropping the explicit dependence on the parameters and model for the sake of conciseness)

$$
\begin{aligned}
-2\nabla_\theta\log\mathcal{L} &= \nabla_\theta\sum_{p,q}\left[\Phi_{pq}^{\mathrm{d}}\left(\hat{\Phi}^{-1}\right)_{qp}\right] + \nabla_\theta\log\left|\hat{\Phi}\right| = \\
&= \sum_{p,q}\left[\Phi_{pq}^{\mathrm{d}}\nabla_\theta\left(\hat{\Phi}^{-1}\right)_{qp} + \left(\hat{\Phi}^{-1}\right)_{pq}\nabla_\theta\hat{\Phi}_{qp}\right] = \\
&= \sum_{p,q,r,s}\left[-\Phi_{pq}^{\mathrm{d}}\left(\hat{\Phi}^{-1}\right)_{qr}\nabla_\theta\hat{\Phi}_{rs}\left(\hat{\Phi}^{-1}\right)_{sp} + \left(\hat{\Phi}^{-1}\right)_{pq}\hat{\Phi}_{qr}\left(\hat{\Phi}^{-1}\right)_{rs}\nabla_\theta\hat{\Phi}_{sp}\right] = \\
&= \sum_{p,q,r,s}\left[\left(\hat{\Phi}^{-1}\right)_{pq}\left(\hat{\Phi}_{qr} - \Phi_{qr}^{\mathrm{d}}\right)\left(\hat{\Phi}^{-1}\right)_{rs}\nabla_\theta\hat{\Phi}_{sp}\right] = 0,
\end{aligned}
\tag{A.5}
$$

where for any square matrix A, $\sum_{i,j}A_{ij}A_{ji} = \mathrm{Tr}\,[AA]$ (with 'Tr' denoting the trace operator), and we have used the following properties:

$$
\begin{aligned}
\nabla_\theta|A| &= \sum_{i,j}\left[\mathrm{adj}(A)_{ij}\nabla_\theta A_{ji}\right] = |A|\sum_{i,j}\left[\left(A^{-1}\right)_{ij}\nabla_\theta A_{ji}\right], \\
\nabla_\theta A^{-1} &= -A^{-1}\nabla_\theta A A^{-1},
\end{aligned}
\tag{A.6}
$$

where $\mathrm{adj}(A)$ is the adjugate of the matrix A. Using the same matrix properties as in Equation (3.4), we can write the maximization condition as

$$
-2\nabla_\theta\log\mathcal{L} \propto \sum_{i,j}\nabla_\theta\hat{\Psi}_i\left(\mathrm{Cov}^{-1}\right)_{ij}\left(\Psi_j^{\mathrm{d}} - \hat{\Psi}_j\right) = 0,
\tag{A.7}
$$

which is the same condition as for the Gaussian likelihood of Equation (2.1). Therefore, at any order in the expansion of the observable on the parameters, the results found in Equation (2.5) also apply for the likelihood of Wishart distributed variables. This is because the two likelihoods share the same best-fit parameters, even if the distributions are different.

B Systematic bias as function of the largest scales included

In our analysis, we have found that, in most cases, the bias due to neglecting lensing magnification or using the Limber approximation is more significant when $\ell_{\max} = 200$ is set (see e.g.,
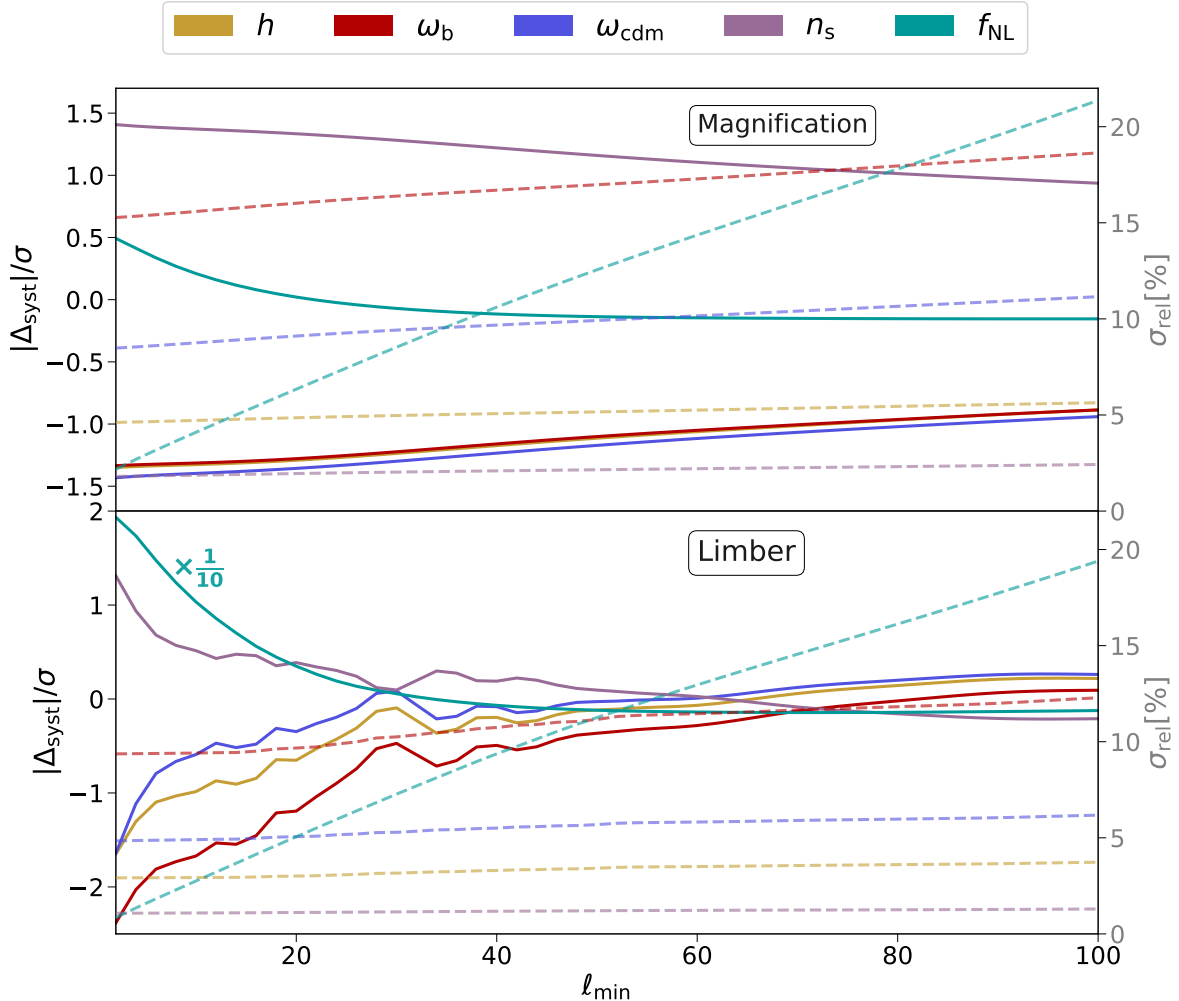
Figure 8: Ratio of the estimated bias in the cosmological parameters over the forecasted 68% confidence level marginalized constraints (solid lines, left side y-axis) compared to the relative forecasted 68% confidence level marginalized constraints – except for f_{NL}, for which we show the absolute forecasted constraint – (dashed lines, right side y-axis), both of them as function of the minimum multipole $\ell_{\min}$ included in the analysis. We show results for the case when the lensing magnification is not modeled (upper panel) and the Limber approximation is used (bottom panel), considering the combination of an Euclid-like survey and a SPHEREx-like survey performing a multi-tracer analysis. In all cases we consider $s = 0.6$ for both galaxy populations, and $\ell_{\max}(z)$. Note that in the lower panel, the result corresponding to $\Delta_{\mathrm{syst},f_{\mathrm{NL}}}/\sigma_{f_{\mathrm{NL}}}$ is divided by a factor 10 for visualization purposes.

Figures 1 and 6). This is because these two approximations are increasingly less accurate at low ℓ. Although we advocate the use of accurate approximations throughout and exploit the whole set of observations (instead of limiting the extent of the analysis to a regime where approximations hold), it is interesting to explore how the significance of the bias decreases as we reduce the multipole range included in the analysis by increasing the minimum multipole $\ell_{\min}$. The expected reduction of the significance of the bias is due to a smaller $\Delta_{\mathrm{syst},a}$ – because the data for which the approximation is less accurate are not included – and due to

an increase in σ_a – given that we are using less data –.

In Figure 8, we compare $\Delta_{\mathrm{syst},a}/\sigma_a$ and σ_a/a (y-axis legend on the left and right side of each panel, respectively) as a function $\ell_{\min}$ for our default choice of $\ell(z)$. We show estimations for the five cosmological parameters considered, for the multi-tracer case, and both for the case where lensing magnification is neglected (upper panel) and the Limber approximation is used (bottom panel). For the case in which lensing magnification is neglected, increasing $\ell_{\min}$ does not reduce significantly the biases in the inferred parameters, while for the case in which the Limber approximation is used, the systematic errors are below $\sim 0.5\sigma$ for $\ell_{\min} \gtrsim 60$. However, in both cases, the constraining power on f_{NL} (one of the main scientific targets of the next-generation galaxy surveys) quickly degrades as we increase $\ell_{\min}$.

We want to emphasize that this discussion is mostly for illustration purposes, and that it is certainly desirable to adopt accurate approximations for the data available, rather than discarding data to be able to use inferior approximations. Moreover, in the case of pursuing a constraint on f_{NL}, using as much data as possible on the largest scales is key.

References

[1] Planck Collaboration, N. Aghanim, Y. Akrami, M. Ashdown, J. Aumont, C. Baccigalupi, et al., "Planck 2018 results. VI. Cosmological parameters", ArXiv e-prints (July, 2018) , arXiv:1807.06209.

[2] The **SDSS-III BOSS**, S. Alam et al., "The clustering of galaxies in the completed SDSS-III Baryon Oscillation Spectroscopic Survey: cosmological analysis of the DR12 galaxy sample", MNRAS **470** (Sept., 2017) 2617–2652, arXiv:1607.03155.

[3] D. M. Scolnic, D. O. Jones, A. Rest, Y. C. Pan, et al., "The Complete Light-curve Sample of Spectroscopically Confirmed SNe Ia from Pan-STARRS1 and Cosmological Constraints from the Combined Pantheon Sample", Astrophys. J. **859** no. 2, (Jun, 2018) 101, arXiv:1710.00845 [astro-ph.CO].

[4] T. M. C. Abbott, F. B. Abdalla, A. Alarcon, J. Aleksić, S. Allam, S. Allen, A. Amara, J. Annis, J. Asorey, S. Avila, D. Bacon, E. Balbinot, and Dark Energy Survey Collaboration, "Dark Energy Survey year 1 results: Cosmological constraints from galaxy clustering and weak lensing", PRD **98** no. 4, (Aug, 2018) 043526, arXiv:1708.01530 [astro-ph.CO].

[5] L. Verde, T. Treu, and A. G. Riess, "Tensions between the early and late Universe", Nature Astronomy **3** (Sep, 2019) 891–895, arXiv:1907.10625 [astro-ph.CO].

[6] A. G. Riess, S. Casertano, W. Yuan, L. M. Macri, and D. Scolnic, "Large Magellanic Cloud Cepheid Standards Provide a 1% Foundation for the Determination of the Hubble Constant and Stronger Evidence for Physics beyond ΛCDM", Astrophys. J **876** no. 1, (May, 2019) 85, arXiv:1903.07603 [astro-ph.CO].

[7] K. C. Wong, S. H. Suyu, G. C. F. Chen, C. E. Rusu, M. Millon, D. Sluse, V. Bonvin, C. D. Fassnacht, S. Taubenberger, M. W. Auger, S. Birrer, J. H. H. Chan, F. Courbin, S. Hilbert, O. Tihhonova, T. Treu, A. Agnello, X. Ding, I. Jee, E. Komatsu, A. J. Shajib, A. Sonnenfeld, R. D. Bland ford, L. V. E. Koopmans, P. J. Marshall, and G. Meylan, "H0LiCOW XIII. A 2.4% measurement of H_0 from lensed quasars: 5.3σ tension between early and late-Universe probes", arXiv e-prints (Jul, 2019) arXiv:1907.04869, arXiv:1907.04869 [astro-ph.CO].

[8] H. Hildebrandt, F. Köhlinger, J. L. van den Busch, B. Joachimi, C. Heymans, A. Kannawadi, A. H. Wright, M. Asgari, C. Blake, H. Hoekstra, and S. Joudaki, "KiDS+VIKING-450: Cosmic shear tomography with optical+infrared data", arXiv e-prints (Dec, 2018) arXiv:1812.06076, arXiv:1812.06076 [astro-ph.CO].

[9] R. P. Norris et al., "EMU: Evolutionary Map of the Universe", PASA **28** (Aug., 2011) 215–248, `arXiv:1106.3219`.

[10] DESI Collaboration, A. Aghamousa, and et al., "The DESI Experiment Part I: Science,Targeting, and Survey Design", ArXiv e-prints (Oct., 2016) , `arXiv:1611.00036 [astro-ph.IM]`.

[11] L. Amendola, S. Appleby, A. Avgoustidis, D. Bacon, T. Baker, et al., "Cosmology and fundamental physics with the Euclid satellite", Living Reviews in Relativity **21** no. 1, (Apr, 2018) 2, `arXiv:1606.00180 [astro-ph.CO]`.

[12] The **LSST Science Collaborations**, P. A. Abell et al., "LSST Science Book, Version 2.0", `arXiv:0912.0201`.

[13] Square Kilometre Array Cosmology Science Working Group, D. J. Bacon, et al., "Cosmology with Phase 1 of the Square Kilometre Array Red Book 2018: Technical specifications and performance forecasts", PASA **37** (Jan., 2020) e007, `arXiv:1811.02743 [astro-ph.CO]`.

[14] O. Doré, J. Bock, M. Ashby, P. Capak, A. Cooray, et al., "Cosmology with the SPHEREX All-Sky Spectral Survey", arXiv e-prints (Dec, 2014) arXiv:1412.4872, `arXiv:1412.4872 [astro-ph.CO]`.

[15] D. J. Watts, B. Wang, A. Ali, J. W. Appel, C. L. Bennett, D. T. Chuss, S. Dahal, J. R. Eimer, T. Essinger-Hileman, K. Harrington, G. Hinshaw, J. Iuliano, T. A. Marriage, N. J. Miller, I. L. Padilla, L. Parker, M. Petroff, K. Rostem, E. J. Wollack, and Z. Xu, "A Projected Estimate of the Reionization Optical Depth Using the CLASS Experiment's Sample Variance Limited E-mode Measurement", Astrophys. J. **863** (Aug., 2018) 121, `arXiv:1801.01481`.

[16] P. Ade, , and The Simons Observatory collaboration, "The Simons Observatory: science goals and forecasts", JCAP **2019** no. 2, (Feb, 2019) 056, `arXiv:1808.07445 [astro-ph.CO]`.

[17] K. N. Abazajian et al., "CMB-S4 Science Book, First Edition", arXiv e-prints (Oct, 2016) arXiv:1610.02743, `arXiv:1610.02743 [astro-ph.CO]`.

[18] E. D. Kovetz, M. P. Viero, A. Lidz, L. Newburgh, M. Rahman, E. Switzer, M. Kamionkowski, et al., "Line-Intensity Mapping: 2017 Status Report", arXiv e-prints (Sep, 2017) arXiv:1709.09066, `arXiv:1709.09066 [astro-ph.CO]`.

[19] E. D. Kovetz, P. C. Breysse, A. Lidz, J. Bock, C. M. Bradford, T.-C. Chang, S. Foreman, H. Padmanabhan, A. Pullen, D. Riechers, M. B. Silva, and E. Switzer, "Astrophysics and Cosmology with Line-Intensity Mapping", arXiv e-prints (Mar., 2019) , `arXiv:1903.04496`.

[20] J. L. Bernal, P. C. Breysse, H. Gil-Marín, and E. D. Kovetz, "A User's Guide to Extracting Cosmological Information from Line-Intensity Maps", arXiv e-prints (Jul, 2019) arXiv:1907.10067, `arXiv:1907.10067 [astro-ph.CO]`.

[21] J. L. Bernal, P. C. Breysse, and E. D. Kovetz, "The Cosmic Expansion History from Line-Intensity Mapping", arXiv e-prints (Jul, 2019) arXiv:1907.10065, `arXiv:1907.10065 [astro-ph.CO]`.

[22] J. B. Muñoz, "A Standard Ruler at Cosmic Dawn", arXiv e-prints (Apr, 2019) arXiv:1904.07868, `arXiv:1904.07868 [astro-ph.CO]`.

[23] A. F. Heavens, T. D. Kitching, and L. Verde, "On model selection forecasting, dark energy and modified gravity", MNRAS **380** no. 3, (Sep, 2007) 1029–1035, `arXiv:astro-ph/0703191 [astro-ph]`.

[24] A. N. Taylor, T. D. Kitching, D. J. Bacon, and A. F. Heavens, "Probing dark energy with the shear-ratio geometric test", MNRAS **374** no. 4, (Feb., 2007) 1377–1403, `arXiv:astro-ph/0606416 [astro-ph]`.

[25] C. A. J. Duncan, B. Joachimi, A. F. Heavens, C. Heymans, and H. Hildebrandt, "On the

complementarity of galaxy clustering with cosmic shear and flux magnification", MNRAS **437** no. 3, (Jan., 2014) 2471–2487, arXiv:1306.6870 [astro-ph.CO].

[26] L. Knox, R. Scoccimarro, and S. Dodelson, "Impact of Inhomogeneous Reionization on Cosmic Microwave Background Anisotropy", Phys. Rev. Letters **81** no. 10, (Sept., 1998) 2004–2007, arXiv:astro-ph/9805012 [astro-ph].

[27] D. Huterer, "Weak lensing and dark energy", Phys. Rev. D **65** no. 6, (Mar., 2002) 063001, arXiv:astro-ph/0106399 [astro-ph].

[28] D. Huterer and M. Takada, "Calibrating the nonlinear matter power spectrum: Requirements for future weak lensing surveys", Astroparticle Physics **23** no. 4, (May, 2005) 369–376, arXiv:astro-ph/0412142 [astro-ph].

[29] D. Huterer, M. Takada, G. Bernstein, and B. Jain, "Systematic errors in future weak-lensing surveys: requirements and prospects for self-calibration", MNRAS **366** no. 1, (Feb., 2006) 101–114, arXiv:astro-ph/0506030 [astro-ph].

[30] A. Amara and A. Réfrégier, "Systematic bias in cosmic shear: extending the Fisher matrix", MNRAS **391** no. 1, (Nov., 2008) 228–236, arXiv:0710.5171 [astro-ph].

[31] A. Natarajan, A. R. Zentner, N. Battaglia, and H. Trac, "Systematic errors in the measurement of neutrino masses due to baryonic feedback processes: Prospects for stage IV lensing surveys", Phys. Rev. D **90** no. 6, (Sep, 2014) 063516, arXiv:1405.6205 [astro-ph.CO].

[32] A. G. Kim, E. V. Linder, R. Miquel, and N. Mostek, "Effects of systematic uncertainties on the supernova determination of cosmological parameters", MNRAS **347** no. 3, (Jan., 2004) 909–920, arXiv:astro-ph/0304509 [astro-ph].

[33] A. Taruya, T. Nishimichi, and S. Saito, "Baryon acoustic oscillations in 2D: Modeling redshift-space power spectrum from perturbation theory", Phys. Rev. D **82** no. 6, (Sep, 2010) 063522, arXiv:1006.0699 [astro-ph.CO].

[34] A. R. Pullen, C. M. Hirata, O. Doré, and A. Raccanelli, "Interloper bias in future large-scale structure surveys", Pub. of the Astron. Soc. of Japan **68** no. 1, (Feb, 2016) 12, arXiv:1507.05092 [astro-ph.CO].

[35] S. Camera, R. Maartens, and M. G. Santos, "Einstein's legacy in galaxy surveys.", MNRAS **451** (July, 2015) L80–L84, arXiv:1412.4781 [astro-ph.CO].

[36] W. Cardona, R. Durrer, M. Kunz, and F. Montanari, "Lensing convergence and the neutrino mass scale in galaxy redshift surveys", Phys. Rev. D **94** no. 4, (Aug., 2016) 043007, arXiv:1603.06481 [astro-ph.CO].

[37] C. S. Lorenz, D. Alonso, and P. G. Ferreira, "Impact of relativistic effects on cosmological parameter estimation", Phys. Rev. D **97** no. 2, (Jan., 2018) 023537, arXiv:1710.02477 [astro-ph.CO].

[38] G. Jelic-Cizmek, F. Lepori, C. Bonvin, and R. Durrer, "On the importance of lensing for galaxy clustering in photometric and spectroscopic surveys", arXiv e-prints (Apr., 2020) arXiv:2004.12981, arXiv:2004.12981 [astro-ph.CO].

[39] A. Raccanelli, L. Verde, and F. Villaescusa-Navarro, "Biases from neutrino bias: to worry or not to worry?", MNRAS **483** no. 1, (Feb, 2019) 734–743, arXiv:1704.07837 [astro-ph.CO].

[40] A. Taylor, B. Joachimi, and T. Kitching, "Putting the precision in precision cosmology: How accurate should your data covariance matrix be?", MNRAS **432** no. 3, (July, 2013) 1928–1946, arXiv:1212.4359 [astro-ph.CO].

[41] D. Kodwani, D. Alonso, and P. Ferreira, "The effect on cosmological parameter estimation of a parameter dependent covariance matrix", The Open Journal of Astrophysics **2** no. 1, (Mar., 2019) 3, arXiv:1811.11584 [astro-ph.CO].

[42] E. Sellentin and A. F. Heavens, "On the insufficiency of arbitrarily precise covariance matrices: non-Gaussian weak-lensing likelihoods", MNRAS **473** no. 2, (Jan., 2018) 2355–2363, arXiv:1707.04488 [astro-ph.CO].

[43] M. S. Wang, W. J. Percival, S. Avila, R. Crittenden, and D. Bianchi, "Cosmological inference from galaxy-clustering power spectrum: Gaussianization and covariance decomposition", MNRAS **486** no. 1, (June, 2019) 951–965, arXiv:1811.08155 [astro-ph.CO].

[44] N. Bellomo, J. L. Bernal, G. Scelfo, A. Raccanelli, and L. Verde, "Beware of commonly used approximations I: errors in forecasts", JCAP **2020** no. 10, (2020) 016, arXiv:2005.10384 [astro-ph.CO].

[45] J. Lesgourgues, "The Cosmic Linear Anisotropy Solving System (CLASS) I: Overview", arXiv:1104.2932 [astro-ph.IM].

[46] D. Blas, J. Lesgourgues, and T. Tram, "The Cosmic Linear Anisotropy Solving System (CLASS) II: Approximation schemes", JCAP **1107** (2011) 034, arXiv:1104.2933 [astro-ph.CO].

[47] R. A. Fisher, "The Fiducial Argument in Statistical Inference", Annals Eugen. **6** (1935) 391–398.

[48] M. Schmittfull, M. Simonović, V. Assassi, and M. Zaldarriaga, "Modeling Biased Tracers at the Field Level", arXiv e-prints (Nov, 2018) arXiv:1811.10640, arXiv:1811.10640 [astro-ph.CO].

[49] D. Ginzburg, V. Desjacques, and K. C. Chan, "Shot noise and biased tracers: A new look at the halo model", Phys. Rev. D **96** no. 8, (Oct, 2017) 083528, arXiv:1706.08738 [astro-ph.CO].

[50] F. Montanari and R. Durrer, "Measuring the lensing potential with tomographic galaxy number counts", JCAP **2015** no. 10, (Oct., 2015) 070, arXiv:1506.01369 [astro-ph.CO].

[51] M. Tegmark, A. N. Taylor, and A. F. Heavens, "Karhunen-Loève Eigenvalue Problems in Cosmology: How Should We Tackle Large Data Sets?", Astrophys. J. **480** (May, 1997) 22–35, astro-ph/9603021.

[52] S. Hamimeche and A. Lewis, "Likelihood analysis of CMB temperature and polarization power spectra", Phys. Rev. D **77** (May, 2008) 103013, arXiv:0801.0554.

[53] A. Raccanelli, O. Doré, and N. Dalal, "Optimization of spectroscopic surveys for testing non-Gaussianity", JCAP **8** (Aug., 2015) 034, arXiv:1409.1927.

[54] A. Raccanelli, M. Shiraishi, N. Bartolo, D. Bertacca, M. Liguori, S. Matarrese, R. P. Norris, and D. Parkinson, "Future constraints on angle-dependent non-Gaussianity from large radio surveys", Physics of the Dark Universe **15** (Mar., 2017) 35–46.

[55] E.-M. Mueller, W. J. Percival, and R. Ruggeri, "Optimizing primordial non-Gaussianity measurements from galaxy surveys", MNRAS **485** (May, 2019) 4160–4166, arXiv:1702.05088.

[56] J. L. Bernal, A. Raccanelli, E. D. Kovetz, D. Parkinson, R. P. Norris, G. Danforth, and C. Schmitt, "Probing ΛCDM cosmology with the Evolutionary Map of the Universe survey", JCAP **2019** no. 2, (Feb, 2019) 030, arXiv:1810.06672 [astro-ph.CO].

[57] D. Karagiannis, A. Lazanu, M. Liguori, A. Raccanelli, N. Bartolo, and L. Verde, "Constraining primordial non-Gaussianity with bispectrum and power spectrum from upcoming optical and radio surveys", MNRAS **478** no. 1, (July, 2018) 1341–1376, arXiv:1801.09280 [astro-ph.CO].

[58] S. Matarrese, L. Verde, and R. Jimenez, "The Abundance of High-Redshift Objects as a Probe of Non-Gaussian Initial Conditions", Astrophys. J. **541** (Sept., 2000) 10–24, astro-ph/0001366.

[59] N. Dalal, O. Doré, D. Huterer, and A. Shirokov, "Imprints of primordial non-Gaussianities on large-scale structure: Scale-dependent bias and abundance of virialized objects", Phys. Rev. D

77 no. 12, (June, 2008) 123514, `arXiv:0710.4560`.

[60] S. Matarrese and L. Verde, "The Effect of Primordial Non-Gaussianity on Halo Bias", Astrophys. J. Letters **677** (Apr., 2008) L77, `arXiv:0801.4826`.

[61] V. Desjacques and U. Seljak, "Primordial non-Gaussianity from the large-scale structure", Classical and Quantum Gravity **27** no. 12, (June, 2010) 124011, `arXiv:1003.5020`.

[62] M. Grossi, L. Verde, C. Carbone, K. Dolag, E. Branchini, F. Iannuzzi, S. Matarrese, and L. Moscardini, "Large-scale non-Gaussian mass function and halo bias: tests on N-body simulations", MNRAS **398** no. 1, (Sept., 2009) 321–332, `arXiv:0902.2013 [astro-ph.CO]`.

[63] C. Wagner and L. Verde, "N-body simulations with generic non-Gaussian initial conditions II: halo bias", JCAP **2012** no. 3, (Mar., 2012) 002, `arXiv:1102.3229 [astro-ph.CO]`.

[64] J. Yoo, A. L. Fitzpatrick, and M. Zaldarriaga, "New perspective on galaxy clustering as a cosmological probe: General relativistic effects", Phys. Rev. D **80** no. 8, (Oct., 2009) 083514, `arXiv:0907.0707 [astro-ph.CO]`.

[65] J. Yoo, "General relativistic description of the observed galaxy power spectrum: Do we understand what we measure?", Phys. Rev. D **82** no. 8, (Oct., 2010) 083508, `arXiv:1009.3021`.

[66] C. Bonvin and R. Durrer, "What galaxy surveys really measure", Phys. Rev. D **84** (Sept., 2011) 063505.

[67] A. Challinor and A. Lewis, "Linear power spectrum of observed source number counts", Phys. Rev. D **84** (Aug., 2011) 043516.

[68] D. Jeong, F. Schmidt, and C. M. Hirata, "Large-scale clustering of galaxies in general relativity", Phys. Rev. D **85** no. 2, (Jan., 2012) 023504, `arXiv:1107.5427`.

[69] D. Bertacca, R. Maartens, A. Raccanelli, and C. Clarkson, "Beyond the plane-parallel and Newtonian approach: wide-angle redshift distortions and convergence in general relativity", JCAP **10** (Oct., 2012) 025, `arXiv:1205.5221`.

[70] A. Raccanelli, F. Montanari, D. Bertacca, O. Doré, and R. Durrer, "Cosmological measurements with general relativistic galaxy correlations", JCAP **2016** (May, 2016) 009.

[71] A. Raccanelli, D. Bertacca, R. Maartens, C. Clarkson, and O. Doré, "Lensing and time-delay contributions to galaxy correlations", General Relativity and Gravitation **48** (July, 2016) 84.

[72] H. Hildebrandt, "Observational biases in flux magnification measurements", MNRAS **455** no. 4, (Feb., 2016) 3943–3951, `arXiv:1511.01352 [astro-ph.GA]`.

[73] L. van Waerbeke, "Shear and magnification: cosmic complementarity", MNRAS **401** no. 3, (Jan., 2010) 2093–2100, `arXiv:0906.1583 [astro-ph.CO]`.

[74] B. Casaponsa, A. F. Heavens, T. D. Kitching, L. Miller, R. B. Barreiro, and E. Martínez-González, "Size magnification as a complement to cosmic shear", MNRAS **430** no. 4, (Apr., 2013) 2844–2853, `arXiv:1209.1646 [astro-ph.CO]`.

[75] E. L. Turner, J. P. Ostriker, and J. R. Gott, III, "The statistics of gravitational lenses - The distributions of image angular separations and lens redshifts", Astrophysical Journal **284** (Sep, 1984) 1–22.

[76] M. Bartelmann and P. Schneider, "Weak gravitational lensing", Phyics Reporst **340** (Jan., 2001) 291–472.

[77] D. N. Limber, "The Analysis of Counts of the Extragalactic Nebulae in Terms of a Fluctuating Density Field", Astrophysical Journal **117** (1953) 134.

[78] N. Kaiser, "Weak Lensing and Cosmology", The Astrophysical Journal **498** no. 1, (1998) 26, `arXiv:astro-ph/9610120`.

[79] M. LoVerde and N. Afshordi, "Extended Limber approximation", Phys. Rev. D **78** (Dec, 2008)

123506, `arXiv:0809.5112`.

[80] X. Fang, E. Krause, T. Eifler, and N. MacCrann, "Beyond Limber: efficient computation of angular power spectra for galaxy clustering and weak lensing", JCAP **2020** no. 5, (May, 2020) 010, `arXiv:1911.11947 [astro-ph.CO]`.

[81] U. Seljak, "Extracting Primordial Non-Gaussianity without Cosmic Variance", Physical Review Letters **102** no. 2, (Jan., 2009) 021302, `arXiv:0807.1770`.

[82] P. McDonald and U. Seljak, "How to evade the sample variance limit on measurements of redshift-space distortions", JCAP **10** (Oct., 2009) 007, `arXiv:0810.0323`.

[83] J. L. Bernal, T. L. Smith, K. K. Boddy, and M. Kamionkowski, "Robustness of baryon acoustic oscillations constraints to beyond-ΛCDM cosmologies", arXiv e-prints (Apr., 2020) arXiv:2004.07263, `arXiv:2004.07263 [astro-ph.CO]`.

[84] B. Joachimi and A. N. Taylor, "Forecasts of non-Gaussian parameter spaces using Box–Cox transformations", Monthly Notices of the Royal Astronomical Society **416** no. 2, (2011) 1010–1022, `arXiv:1103.3370`.

[85] E. Sellentin, M. Quartin, and L. Amendola, "Breaking the spell of Gaussianity: forecasting with higher order Fisher matrices", MNRAS **441** (June, 2014) 1831–1840, `arXiv:1401.6892`.

[86] E. Sellentin, "A fast, always positive definite and normalizable approximation of non-Gaussian likelihoods", Monthly Notices of the Royal Astronomical Society **453** no. 1, (2015) 893–898, `arXiv:1506.04866`.

[87] L. Amendola and E. Sellentin, "Optimizing parameter constraints: a new tool for Fisher matrix forecasts", Monthly Notices of the Royal Astronomical Society **457** no. 2, (2016) 1490–1495, `arXiv:1602.01746`.